Trace and rare earth element geochemistry of the Oligocene Nikopol stratiform manganese oxide-hydroxide ores, Ukraine

Ahmet Sasmaz[a*], Vasyl M. Zagnitko[b], Bilge Sasmaz[a]

[a*] Department of Geological Engineering, Firat University 23119, Elazig, Turkey

[b] Taras Shevchenko National University of Kyiv, Institute of Geology, 90 Vasylkivska, Kiev, Ukraine

Abstract

The Nikopol manganese deposit is one of the world's largest deposits among the sedimentary manganese deposits. The Nikopol Oligocene basin is located between the Azov crystalline massif and the Ukrainian shield. Nikopol Ore horizon is traced in a thickness varying from several cm to 4.5 m and a single stratum from the west to the eastwards to about 250 km and separated to three different units; carbonate, mixed carbonate-oxide, and oxide ore. The oxide ores can contain the concretion or earthy masses bigger than 25 cm, sometimes with remnants of carbonate or carbonate-oxide textures. The manganese oxide-hydroxide ores were analyzed for major oxides, trace and rare earth elements (REE) using ICP-MS. The PAAS-normalized REE patterns of the Nikopol manganese oxide ores have similar trends and show MREE and HREEs enrichments. The Ce/Ce* values of manganese oxide-hydroxide ores collected from the study area vary from 0.88 to 1.43, indicating that ore-forming rocks were primarily marine chemical or biogenic deposit. The Eu/ Eu* anomalies of the manganese oxide-hydroxide ores are close to 1. The Y concentrations vary from 9,1 to 47,1 ppm and show negative Y anomalies. Both geochemical and Pb isotope data indicate that the Nikopol manganese oxide-hydroxide ores formed rapidly within oxic/suboxic seawater as reflected by Ce anomalies close to 1 in low-oxygen fugacity in source of the hydrothermal fluids, volcanogenic input or hydrothermal contributions to seawater. Also, our results point out that the metal was transported from both a hydrothermal source in deeper water and terrestrial sources.

Key words: Manganese oxide ore, trace element, rare earth element, Nikopol, Ukraine

Plain Language Summary

Manganese occurs in many minerals such as manganite, sugilite, purpurite, rhodonite, rhodochrosite, and pyrolusite. The most important use of manganese is in the manufacturing of steel. Currently, steel production accounts for 85 to 90% of total manganese consumption. Manganese is often used by the steel industry in deoxidizing, desulfurizing additives and dry cell batteries. It can improve the rolling and forging qualities, as well as the strength, toughness, stiffness, hardness, wear resistance, and hardenability of steels. As a result, manganese is one of the indispensable elements of technology and will continue to be widely used in the future. For this reason, manganese beds will become much more important in the coming years. Sedimentary manganese deposits produce the bulk

of the world's output of manganese. These deposits in Ukraine, Georgia and Russia are the world leader in manganese ore production with about 45% of world production. Approximately 75% of this came from the Nikopol in the Ukraine and much of remainder from the Chiatura Basin in Georgia. For these reasons, it becomes clear how important the investigation of Nikopol sedimentary manganese deposits is.

1. INTRODUCTION

The Nikopol manganese deposits are located in the Eastern Paratethys basin the Nikopol, at the southeast of Ukraine and one of the largest manganese deposits of metallurgical manganese in the world among the sedimentary manganese deposits. The deposits were discovered in 1883 and production began in 1886 and the total area of explored deposits is about 500 km^2. The ore body is almost horizontal or with a slight (up to 5^0) dips south or southwest. The ore is at 10- to 100-m depth. The thickness of ore varies from 0.5 to 5 m, and on the average is 1.5 to 2.5 m thick. The manganese ore layer is characterized by inter stratification of the ore with sand-silt clay sediments. The estimated total reserves of manganese ore around the Nikopol are calculated to be 626 million tons with grades between 10 and 45% in oxide ore, up to 30% in carbonate ore (Strishkov and Levine, 1987). These deposits are known such giant deposits as Nikopol, Tokmak, Chiatura, Varna, Mangyshlak, Binkilic, Laba, small deposits of Hungary and Slovakia formed in regional palaeogeographic setting of the Early Oligocene of the Eastern Paratethys (Fig 1) (Kuleshov, 2017).

Based on the chemical composition and geological settings of Fe-Mn deposits, they can be divided to three main groups: diagenetic, hydrogenetic, and hydrothermal (Hein et al., 1997; Bau et al., 2014; Josso et al., 2017). Mn-Fe oxides form along the rock surfaces in the global ocean or sea at water depths between 400 and 7000 m. They extremely slowly develop by the collecting of colloids onto rock surfaces and the precipitation of metals from bottom sea water, or by a contribution of hydrothermal and hydrogenetic precipitation in hydrothermal vent areas (Hein et al., 2000). Manganese minerals in sedimentary environments may contain the rare earth element (REE) concentrations in different rates (Chakhmouradian and Wall, 2012) due to ion substitutions (Dill et al., 2011) or through sorption on Mn oxides. Manganese deposits and their REE geochemistry have been used to better understand the geochemical and sedimentological conditions during the formation of manganese minerals and their host rocks (McLennan, 1989; Dubinin, 2006; Hein et al., 2013; Hein and Koschinsky, 2014; Sasmaz et al., 2014; Hein et al., 2017; Konstantinova et al., 2017; Chen et al., 2018; Vereshchagin et al., 2019). The REE concentration in manganese deposits has been extensively used to determine the genesis of hydrothermal systems and the physicochemical parameters of depositional environments (Roy et al., 2018; Tobia, 2018; Sinanoglu and Sasmaz, 2019) in various depositional settings (Akgul, 2015; Sasmaz et al., 2018). The Oligocene manganese oxide deposits in Nikopol and Chiatura contains the main reserves of the world’s onshore reserves of manganese (Maynard, 1983). The petrography and mineralogy of both deposits were extensively studied during the Soviet Union period by various researchers (Varentsov and Rakhmanov, 1980; Bolton and Frakes, 1985; Hein and Bolton, 1994) but no geochemical data

about trace and rare earth element contents were provided for these deposits. Here, we investigated the physico-chemical conditions, the conditions of formation of the Nikopol manganese oxide/hydroxide deposit, and the abundances of major oxide, trace elements, and REE concentration at various levels within the manganese deposit.

2. GEOLOGICAL SETTING OF THE NIKOPOL MANGANESE DEPOSIT

The Eastern Paratethys contains many manganese deposits such as Ukraine (Tokmak and Nikopol); Georgia (Chiatura and Kvirila); Bulgaria (Varna); Kazakhstan (Mangyshlak); Turkey (Binkilıç); North Caucasus (Laba deposits), Hungary and Slovakia) (Fig. 1). Manganese deposits formed in climatic, facies and paleogeographic environments like Nikopol are also found in other places such as the Northern Ural region, Europe, China, and North America. Nikopol 'and Tokmak deposits have more than 1 billion tons of Mn reserves (Kuleshov, 2017).

The Nikopol Oligocene basin is located in the northeast part of the Black Sea tectonic depression zone between the Azov crystalline massif in the east and the Ukrainian crystalline shield in the north (Fig. 1). Manganese ores in Nikopol basin are formed in the Oligocene coastal-marine sediments related with the stratigraphic sequence of the Black Sea depression (Kuleshov, 2017). Oligocene marine basin is a single basin as structural, stratigraphic, and genetic (Fig. 2). All separate ore-bearing parts in this basin are parts of a same system in Oligocene basin. The Nikopol Oligocene basin consists of two structural stages. These are the crystalline basement rocks with Precambrian and sedimentary cover rocks from the Cretaceous to Quaternary. This sedimentary cover rocks are with slope gradually to south-westerly direction (Fig. 3). The unity and thickness of the sequence increase along this same direction. From the north to the south, the shallow water coastal facies of the continental facies are observed first, and further to the south, deep-sea water facies are observed. Oligocene deposits in the upper Cretaceous-Eocene basin lie on the crystalline basement rocks or their weathering crust (Fig. 3). These deposits consist of three distinct members like a subore sands, Mn ores and supra oreclays from the bottom to upwards. The manganese ore of the Nikopol basin has a single ore level extending from west to east over a distance of about 250 km, with a thickness ranging from a few centimeters to 4.5 m (Fig. 3;4). This layer occurs from a sandstone-clay stratum representing a friable manganese ores and concretional manganese carbonate nodules. The concretion sizes vary to several dozens of centimeters from several millimeters up. Manganese carbonate concretions in a length up to several hundred meters have lensoidal structure with frequently intergrown in the host rocks. Manganese ores consist of either the oxides or carbonates or their mixing of oxides and carbonates. A mineral zonality at the Nikopol' deposits is observed that either along the sequence of the ore body from bottom toward top or in the replacement of oxide ores by carbonate ores in the direction into the depth of the basin from the shore of the Oligocene basin. A typical geological cross section for I and II oxide ore areas of the Nikopol manganese deposit is seen in Fig 2 (Strakhov et al., 1968; taken from Kuleshov, 2017). The common and dominant ore in this basin is carbonate type ore. Carbonate ores form a significant part of the ores in the Nikopol region; especially the main reserves are observed in the Bolshoi Tokmak deposits in the east of this region (Fig. 2). Nikopol manganese ore horizon was

separated to three different units by Vorontsov and Rakhmanov (1977); carbonate ore, mixed carbonate-oxide ore, and oxide ore. The carbonate ore shows in the most distal location from the continent and in two textural changes: nodular-concretionary ores in 1 to 25 cm in diameter in a lumpy - coarse ores that have a clay-silt matrix with highly porous texture. Both manganoan calcite and rhodochrosite are always reported to be very fine-grained and poorly crystalline. The carbonate ore facies show the nodular changes such as fish bones, sponge spicules and diatoms but the lumpy variety does not contain such inclusions.

When approaching from the open sea to the paleoshoreline, this carbonate ore passes toward a mixing carbonate-oxide ore facies. The oxide-carbonate ore facie generally consists of irregular spherical masses of Mn oxide varying between 0.1 and 1 cm in Mn carbonate matrix. The Mn oxide masses are about 25 % of the ore. The oxide ores corroded and replacemented by the carbonate matrix showed that the oxide ores formed earlier than the carbonate matrix. Similar paragenesis relations (Calvert and Price 1970) are observed between the cemented oxide nodules and $MnCO_3^-$ in Scotland. The carbonate masses within this facies have a similar composition with the carbonate facies. The closest regions to the paleo-shoreline consist of manganese oxide ores. The formation of the oxide ores in the paleo-shoreline has been still discussed that these are a deposition of supergene alteration of carbonate ore or the primary oxide ore. Varentsov and Rakhmanov (1977) believe that the carbonate ore and mixed carbonate-oxide ores were only primary. The oxide ores was formed as a result of secondary oxidation of both carbonate and carbonate-oxide ores. The oxide ores in these areas can contain the concretion or earthy masses bigger than 25 cm, sometimes with remnants of carbonate or carbonate-oxide textures (Maynard, 1983). Although the well-developed concentric stratifications are observed here, smaller deformed concretion is often attached to larger aggregates (Maynard, 1983). The main minerals of supergene oxidation zone in Nikopol manganese deposits are: manganite, pyrolusite, todorokite, cryptomelane, birnessi-birnessite, rancieite (Varentsov, 2002).

3. SAMPLES AND ANALYTICAL METHOD

3.1. Sampling

Eleven manganese oxide samples were collected from the oxide-hydroxide zones of Alexandrovsky quarry areas in the Nikopol Mn deposit (Fig 2) for major oxides, trace elements, and rare earth element analyses. As seen in Fig. 4, the oxide ores were sampled toward up from the bottom of the upper manganese ore section. While the bottom part of the cross section generally consists of carbonate ores (with low oxide-hydroxide ores) together with limestone, quartz and clay minerals, the up parts mostly consist of oxide-hydroxide manganese minerals. During sampling, especially manganese oxide-hydroxide samples were collected from the field for the assessment to the geochemistry of trace and rare earth elements. These samples were analyzed separately to detect major oxide, trace and rare earth element contents through this section. In this Fig. 4, the dark parts contains mostly manganese oxide-hydroxide ores and less limestone, quartz and clay minerals, the light sections (yellow and green color) contains mostly limestone, clay minerals, quartz and less manganese piece ore (Fig. 5).

3.2. Analytical Methods

Eleven Mn oxide-hydroxide samples collected from the Nikopol manganese mineralizing area were broken up and after that, were milled to a 200 mesh size for both analyses of major oxides by ICP-AES, and trace and rare earth elements by ICP-MS. In the analyzed samples, the error rate in repeated analyses was reported to be within 5%. The major oxides were analyzed by ICP-AES, trace elements and rare earth elements were analyzed by ICP-MS. All ICP-AES and ICP-MS analyses were performed by Acme Analytical Laboratories in Canada. Powdered manganese samples (50 mg) were firstly digested in a mixture of $HCl:HNO_3:H_2O$ (1:1:1, v/v; 6 ml per 1.0 g of sample) for 1 hour. Then, the major oxide, trace element, and REE analyses in the digested samples were determined by using ICP-AES and ICP-MS in Acme Analytical Laboratory (Canada).

Pb isotope analysis (Pb^{208}, Pb^{207}, Pb^{206}, and Pb^{204}) was performed in manganese oxide/hydroxide samples by the ICP-MS method in Acme Laboratories (Canada). These samples were solved with aqua regia (3HCL + 1 HNO_3 mixture) to analyze $^{206}Pb/^{204}Pb$, $^{207}Pb/^{204}$ Pb and $^{208}Pb/^{204}Pb$ isotope ratios. The NIST-SRM 981 standard was used during the Pb isotope analyses and this standard was 36.7219 for $^{208}Pb/^{204}Pb$, 15.4916 for ^{207}Pb $/^{204}Pb$ value, and 16.9374 for $^{206}Pb/^{204}Pb$ value. For these values repeatability and precision in 8 hour period (error ±% RSD) were calculated as ± 0.27%, ± 0.20% and ± 0.17%.

The corresponding values to calculate Ce, Eu and Y anomalies for each sample were normalized to PAAS by using the formulas (Taylor and McLennan, 1985): $Ce/Ce^* = Ce_n /\sqrt{[La_n * Pr_n]}$, $Eu/ Eu^* = Eu_n /\sqrt{[Sm_n * Gd_n]}$ and $Y/Y^* = Y_n/\sqrt{[Dy_n * Ho_n]}$.

The data were statistically analyzed using the Student Newman Keul's Procedure (SNK) (Sokal and Rohlf, 1995) with SPSS 15.0 software and variance analysis (ANOVA).

3.3. Quality Assurance

Quality Assurance through the process of external auditing by recognized organizations; all facilities maintain ISO registrations and accreditations. These accreditations and registrations meet the requirements of the ISO standards and provide independent verification that the management systems have been implemented. All BVM facilities are registered to ISO 9001 and they are pending to the Bureau Veritas corporate registration. Additionally a number of analytical hubs have received ISO/IEC 17025 accreditation for specific laboratory procedures.

4. RESULTS AND DISCUSSION

4.1. Major Oxide Geochemistry

Major-oxides, loss on ignition (LOI), trace elements, and rare earth element contents analysed by ICP-MS and ICP-AES of 11 manganese oxide-hydroxide samples are given in Table 1. The MnO contents in the Nikopol manganese deposits vary from 32.4 to 54.5 wt% with an average of 40.7%. The major oxide contents of the Nikopol manganese deposits varied from 7.46 to 21.6% for SiO_2, 3.03 to 10.5% for CaO, 2.04 to 6.88% for Al_2O_3, 2.91 to 5.73% for Fe_2O_3 (Table 1). Bivariate plots for n=11, of SiO_2 versus K_2O, SiO_2 versus Al_2O_3 and

184 SiO_2 versus TiO_2 have high positive correlations whereas SiO_2 versus MnO and SiO_2 versus Sr show strong
185 negative correlations. Positive correlations of SiO_2 with K_2O, Al_2O_3 and TiO_2 reflect terrigenous detritus input
186 to the depositional basin. Compared to the Binkılıc (Gultekin and Balci, 2018) and Chiatura manganese
187 deposits, the Nikopol manganese deposit has higher Fe_2O_3 and MgO contents and a lower SiO_2 and Al_2O_3
188 contents for Binkilic and higher contents for Chiatura manganese oxide deposit. Nikopol manganese oxide
189 deposit chemical data are plotted on discrimination diagrams to find the genetic origin and depositional
190 environment (Fig. 5). These diagrams indicate that the Nikopol manganese oxide deposit formed as
191 hydrogenetic precipitates in shallow-marine environments. Strong linear correlations were detected in SiO_2-
192 Al_2O_3, SiO_2- TiO_2, SiO_2- K_2O, TiO_2-K_2O, MnO-P_2O_5, Al_2O_3-K2O and Al_2O_3-TiO_2 whereas negative correlations
193 were observed in MnO-CaO, Al_2O_3-CaO, SiO_2-K_2O, and CaO-Na_2O. These major oxide correlation relations
194 show that MnO transported only to manganese ore area together with P_2O_5, not other major oxides.
195
196 **4.2. Trace Element Geochemistry**
197 The trace element contents of the Nikopol manganese oxide-hydroxide ores, together with some
198 parameters and the detection limits are given in Table 2. The total trace element concentrations in the analysed
199 ores were between 433 and 7897 ppm with a mean of 2836, whereas the average trace element content of
200 marine sediments is 760 ppm (Turekian and Wedepohl, 1961). Average concentrations for the trace elements
201 are V (95 ppm), Co (74 ppm), Ni (101 ppm), Cu (61 ppm), Sr (638 ppm), Y (18.4 ppm), Ba (1709 ppm), As
202 (19,4 ppm), U (11,7 ppm), and Zn (55,4 ppm). The Nikopol manganese ores contain more Co, Ni, Cu, Sr, Ba,
203 As, Cd and U, and lower V, Cr, Rb, Zr, Nb, Hf, Th, Pb and Zn compared to Post Archean Australian Shale
204 (PAAS) (Taylor and McLennan, 1985) (Fig. 6). While the Sr and Ba from the LILE elements are slightly
205 enriched, Zr, Hf, Nb and Rb is strongly depleted in compared to PAAS (Fig 6). The PAAS-normalized
206 ferromanganese-hosted trace elements (Co, Ni and Cu) showed strong enrichments together with As, Ba, and U,
207 except for Pb, Zn, V and Cr (Fig. 6). For the HFSE (Y, Zr, Hf, Nb, U and Th), Nb, Zr, Hf, and Th are highly
208 depleted, except for Sr, Y and U. The average Mn/Fe, Co/Zn, Co/Ni, and Zr/Hf ratios in the Nikopol
209 manganese oxide ores are 25, 0.54, 1.15, and 57, respectively (Table 2).
210 Discrimination diagrams for Mn–Fe–(Ni + Co + Cu)x10 (Bonatti et al., 1972; Crerar et al., 1982) and
211 Zn–Ni–Co (Choi and Hariya, 1992) trace element concentrations in the Nikopol manganese oxide ores indicate
212 the mostly hydrothermal+diagenetic and hydrogenetic origins (Fig. 5).
213 The major oxide and trace element contents for different type manganese deposits in the world are given
214 in Table 3. These contents of the Nikopol manganese deposit are similar with those of the Hazara, Binkilic,
215 Elazig and Chiatura Mn deposits in Turkey (Shah and Moon, 2007; Gultekin and Balci, 2018; Sasmaz et al.,
216 2014) (Table 3). The ratios between Mn and Fe are defined as Mn:Fe = 16.76 (5.38 to 58.31) for the Binkilic
217 sedimentary manganese deposit, Turkey; Mn:Fe = 0.63 for SEDEX manganese deposits around Elazig, Turkey;
218 Mn:Fe 0.1-10 for SEDEX deposits; Mn:Fe = 1 for a hydrogenous origin and Mn:Fe <1 for a lacustrine
219 environment. The Mn:Fe ratios of Nikopol manganese oxide-hydroxide ores vary from between 6.2 and 47
220 (average = 25) (Table 3) and have similar values with Binkilic sedimentary manganese deposits (Gultekin and

Balci, 2018).

The Zr/Hf ratios vary from 33 to 83 with an average of 57 (Table 2). The Nb/Ta ratios range from 2,3 to 8.6 with a mean of 4.13 (Table 2). Fig. 8 shows that the Zr/Hf ratios are similar with North Atlantic Deep Water, Atlantic Fe-Mn crusts and Surface Pacific Fe-Mn crusts and but, the Nb/Ta ratios are lower than for North Atlantic, Pacific, and Southern Ocean Deep Waters (Godfrey et al., 1996, 2009; Firdaus et al., 2011; Schmidt et al., 2014; Censi et al., 2007; 2010; 2017) (Fig 8). The HFSE enrichments in hydrogenetic oxides result from absorption from sea water (Firdaus et al., 2011; Schmidt et al., 2014; Censi et al., 2018; 2019). This also shows that the low Zr/Hf and Nb/Ta ratios in the studied manganese oxide ores indicate a low HFSE content in the seawater during the formation of these manganese oxide-hydroxide ores.

4.3. Rare Earth Element Geochemistry

Table 4 represents the REE+Y concentrations of the Nikopol manganese oxide-hydroxide ores. The average ΣREE concentrations change between 60 ppm and 197 ppm with an average of 108 ppm (Table 4). The Y concentrations vary from 9.1 to 47.1 with average of 18.2 ppm. Shale-normalised patterns of the studied manganese oxide-hydroxide samples (relative to PAAS, Post Archean Australian Shale; Taylor and McLennan, 1995) are reported in Fig 8. The PAAS-normalized REE +Y patterns of these samples followed similar trends to each other and are characterized by a general increase in normalized concentrations along the series, from light REE to heavy REE (Fig. 8). The average REE sequence in the PAAS-normalized REE pattern for the Nikopol manganese oxide-hydroxide ores is as follows: MREE (3,59) > HREE (3.04) > LREE (2,13 (Fig. 8). The La_n/Yb_n ratios are used to determine the enrichment trends for light and heavy REE contents. The La_n/Yb_n ratios of the Nikopol manganese oxide-hydroxide ores ranged between 0.68 and 1.06 with a mean of 0.86, verifying the MREE and HREE enrichments.

Cerium is probably the most efficient element of the REE series to use as a discriminating feature for Fe-Mn deposits. In fact, Ce readily oxidizes and is continuously and irreversibly removed from seawater at the surface of Mn oxides (Takahashi et al., 2007), and therefore positive Ce anomalies in Fe-Mn oxide deposits are considered typical of hydrogenetic deposition. Due to differences in the kinetics among the different Fe-Mn deposits and irreversible Ce uptake from sea water, Ce will be most enriched in hydrogenetic deposits, lower in diagenetic deposits, and lower yet in hydrothermal deposits (Josso et al., 2017). The Ce/Ce* and Eu/Eu* ratios have been used as an indicator of redox state to obtain the physicochemical characteristics of hydrothermal fluids or the depositional environment including fO_2, pH, and temperature (Bau and Möller, 1992; Bau, 1996). The Ce/Ce* values of manganese oxide-hydroxide ores collected from the study area vary from 0.88 to 1.43, with the mean of 1.16, which are positive Ce anomalies ($Ce/Ce^* = Ce_n/\sqrt{[La_n*Pr_n]}$), except for 3 samples, indicating that ore-forming rocks were primarily marine chemical or biogenic deposit (Table 4). Under seawater Eh and pH condition, Ce is primarily Ce^{4+}, its solubility very low, and thus it is not easy to remain dissolved in sea water. It precipitates as Ce^{4+} (CeO_4), causing strong depletion Ce in sea water. The Ce concentrations in the oxide ore are higher than in the primary carbonate ore, because of the redox potential of those two

environments. For example, the seawater shows a strong negative Ce anomaly which is mirrored by a positive anomaly in hydrogenetic ferromanganese crusts and nodules (Elderfield, 1988). However, all the manganese oxide samples had Ce values close to 1 indicative of rapid deposition of the oxide ores and typically lack of enrichment of REE in carbonates. Ce can occur in both the +3 and +4 in oxidation states. Ce (III) in the presence of oxygen is oxidised partially to Ce (IV) on the surface of Mn oxides, where it no longer joins in desorption reactions, leaving seawater depleted in Ce relative to other trivalent REEs. This Ce fractionation only occurs under oxic conditions (German and Elderfield, 1990; German et al., 1991). Negative Ce anomalies can occur in the well-oxygenated modern oceans and indicates rapid deposition of the oxides, not leaving time for the surface oxidation of the Ce (Tostevin et al., 2016). Mn is generally accepted as the main carrier phase for Ce (Bau et al., 2014). Since both Mn and Ce have a high reduction potential, the formation of Ce-enriched Mn oxides needs high dissolved oxygen concentrations based on redox proxies trace elements in the Fe-C-S systems. Local positive Ce anomalies in some modern dissolved Mn-rich develops beneath the Mn (IV/II) redox cline (De Carlo and Green, 2002; De Baar et al., 1988; Bau et al., 1997). This positive Ce anomaly has been reported to occur in late Ediacaran carbonates (Mazumdar et al., 2003), cherts and Fe formations from the Palaeoproterozoic (Slack et al., 2007). This is more likely to inheritance from mineralization of a Mn oxide-hydroxide. Ce anomalies are used as a common redox proxy to speculate on the oxygenation of the marine environment during the Phanerozoic or Precambrian anoxic events (Liu et al., 1988; Bodin et al., 2013; Riding et al., 2014; Tostevin et al., 2016).

Eu anomalies of the manganese oxide-hydroxide ores in the Nikopol are close to 1 ($Eu/ Eu^* = Eu_n /\sqrt{[Sm_n * Gd_n]}$), with a range of 0.68 to 1.12 (mean: 0.96) (Table 3). Six samples have slightly positive Eu anomaly higher than 1, five samples have slightly negative Eu anomaly because of lower than 1. The positive Eu anomalies indicate the existence of Eu^{2+} during deposition and low oxygen fugacity conditions of the hydrothermal solutions. The manganese precipitated from fluids with decreasing temperature or increasing fO_2 or alternatively co-precipitated together with Eu-enriched minerals. Eu anomalies can be related to a few factors, such as increases in pH and fO_2 or decrease in temperature (Ehya, 2012; Deng et al., 2014). Positive Eu anomaly in a PAAS-normalized REE pattern may due to hydrothermal fluids involved in the mineralization (Abedini and Calagari 2015; Tobia 2018). Limestone is generally deposited in a shallow-marine carbonate environment; therefore, local feldspar enrichment in diagenetic environments may also lead to positive Eu anomaly (Roy et al., 2018). Schwinn and Markl (2005) suggested that the reduction of Eu^{3+} to Eu^{2+} occurred at high temperatures which resulted in Eu-enrichment in the minerals relative to the fluids.

Common ternary diagrams do not clearly differentiate Fe-Mn deposits formed by mixed genetic processes (Josso et al., 2017). There are different methods to date which allow us to find out their origins of the Fe-Mn samples based on their trace element compositions (Bau et al., 2014, Josso et al., 2017). The Ce (Ce, Ce/Ce*), Y, Ho, Nd, and Zr concentrations is used as a main tool for investigating the genesis of manganese oxide samples (Bau et al., 2014, Josso et al., 2017). Our samples were plotted on the diagrams along with several typical examples of diagenetic, hydrogenetic, and hydrothermal Fe-Mn deposits (Zeng et al., 2012; Bau et al., 2014; Josso et al, 2017). Both $(Ce/Ce^*)_n$ vs Nd and Ce vs (Co+Ni+Cu)/1000 diagrams in Fig. 9a,b

showed that the Nikopol samples cover similar areas with Baturin (2011) and Vereshchagin et al. (2019)'s samples. Although diagenetic Fe - Mn nodules usually show negative Ce anomaly (Fig 9a), the Nd concentrations in diagenetic manganese have higher concentrations than those of hydrothermal manganese and vary between 10 and 100 ppm (Bau et al., 2014; Vereshchagin et al., 2019). The Ce vs Zr diagram for the Nikopol samples indicated that our samples overlapped in an area between diagenetic and hydrothermal proposed by Bau et al. (2014) (Fig 9c). $Ce/Ce^*)_n$ vs $(Y/Ho)_n$ diagram showed that our samples mostly located within the area of hydrothermal manganese deposits (Fig 9d). The $(Y/Ho)_n$ ratio shows decoupling of the geochemical twins Y and Ho, which produces Y anomalies within REY patterns due to very similar ionic radius to Ho^{3+}, Y^{3+} can be inserted into REE patterns between isovalent Dy^{3+} and Ho^{3+} (Bau, 1996). This decoupling results from preferential scavenging of Ho relative to Y on metal oxide surfaces due to lower stabilities of Y surface complexes (Bau, 1996; Bau, 1999). The Y/Ho values of the manganese oxide-hydroxide ores in the study area vary from 23 to 30, with an average of 26. The REY pattern in anoxic Mediterranean seawater has a negative Ce and positive Y anomalies. The change to a positive anomaly in M-3400 from a negative Ce anomaly in sample M-3200 strongly suggests that in the Tyro sub-basin, similar to the situation in the Bannock sub-basin, Y and REE are involved in the redox-cycling of Mn and Fe (Bau et al., 1997).

The Y concentrations in the Nikopol manganese ores vary from 9,1 to 47,1 ppm, with an average of 18.2 ppm (Table 4). Nikopol manganese oxide-hydroxide samples show negative Y anomalies, except for three samples ($Y/Y^* = Y_n/\sqrt{(Dy_n * Ho_n)}$ between 0.75 and 1.12 with a mean of 0.93 (Table 4). The anoxic water sample shows a REY pattern with considerably less HREE enrichment and less positive Y anomaly in compared to the oxic water. However, the most remarkable variation is the presence of a positive Ce anomaly in the anoxic brine (Bau et al., 1997). These data also show that in environments where manganese deposits are formed, oxic environments from time to time and anoxic environments prevail. Chen et al. (2018) studied the REY geochemistry of the ferromanganese oxides on the eastern flank of the Gagua Ridge collected from a water depth of 4071m. According these results, the REY data, which are normalized to PAAS, exhibited flat patterns with positive Ce anomalies and negative Y anomalies as Nikopol manganese oxide-hydroxide ores.

The Cape Vani (Milos Island, Greece) Mn-oxide and barite deposit shows the three-dimensional characteristics of a shallow-water hydrothermal system between Mn-oxide ores and barite deposits (Hein et al., 1999, 2000). The hydrothermal fluid was predominantly enriched seawater in metals leached from the basement rocks. The hydrothermal solutions were supported by convection driven by heating from a magma source. Mn-oxide mineralization and barite precipitation were syngenetic. We envision that fluids from a similar hydrothermal system contributed to the formation of Chiatura Mn-oxide deposits that combined with the production of Mn-oxides from diagenetic processes, thereby creating a mixed origin ore deposit. It is observed that similar barite and pyrite formations occur with the continuation of Kockale manganese-oxide ore section in Maden Complex (Sasmaz et al., 2014).

4.4. Pb Isotope Geochemistry

The Pb isotope ratios of Nikopol manganese oxide-hydroxide ores are 18.98 for $^{206}Pb/^{204}Pb$, 15.68 for $^{207}Pb/^{204}Pb$ and 39.39 for $^{208}Pb/^{204}Pb$ isotopes (Table 4). According to Wang et al. (2014), The Pb isotope studies in the study area show that Pb in the manganese oxide ores originated from upper crust materials. The $^{207}Pb/^{204}Pb$ isotope ratios vary from 15.64 to 15.73. These values showed that the Nikopol manganese ores were mostly sourced from fluids or metals with upper crust origin (Zartman and Doe, 1981). Pb isotopes values and their potential sources that may support to the seawater Pb isotope composition recorded by Fe-Mn crusts are given in Fig. 10. These ratios indicate that Pb isotope data covered similar areas with the Atlantic crust and pelagic sediments. (Fig 10a,b). These are hydrothermal lead, derived from MORB, continental sources as shown by riverine particulates, island arcs, and young continental margins (von Blanckenburg et al., 1996). The highly radiogenic Pb isotope values in the North Atlantic have been explained by incongruent weathering processes on the old cratonic landmasses of Greenland and northern Canada (von Blanckenburg and Nagler, 2001). The Pb isotope composition of the shallowest crust that grew within the present-day Mediterranean Outflow Water does not show significant Pb isotope changes indicating that it was controlled by the same Pb sources throughout the past 15 Ma. Time series of Pb isotope composition was measured on three ferromanganese crusts recording the evolution of NE Atlantic water masses over the past 15 Ma. The crusts are observed along a depth profile (~700–4600 m) comprising the present-day depths of NE Atlantic Deep Water and Mediterranean Outflow Water. The Pb isotope evolution during the Pliocene-Pleistocene can generally be explained by mixing between two end-members corresponding to NE Atlantic Deep Water and Mediterranean Outflow Water, but Muiños et al. (2008) reported that external sources such as Saharan dust can play an important role in the composition change of waters in this region. Andrieu et al. (1998) investigated that Pb isotope analyses on the basalts and sulfides from the Trans-Atlantic Geotraverse (TAG) hydrothermal site on slow-spreading Mid-Atlantic Ridge (Fig. 10c,d). These data show that the Pb isotope ratios of TAG sulphides reflect the average isotope composition of the upper part of the ocean crust affected by the large-scale hydrothermal fluid circulation, and the sulphides of the Pb isotopic compositions of hydrothermal aeration fluids recorded recently and in the ancient period remain active throughout the active range of a main hydrothermal vent area such as TAG (Andrieu et al., 1998). Fig 10c,d shows that Pb isotope data of Nikopol manganese oxide ores covered the same areas with terrigenous sediments, Mn nodules and pelagic and biogenic sediments.

5. CONCLUSION

The Nikopol manganese deposit located in the Eastern Paratethys basin the Nikopol at the southeast of Ukraine is one of the largest manganese deposits of metallurgical manganese in the world among the sedimentary manganese deposits. The Nikopol Oligocene basin observed between the Azov crystalline massif and the Ukrainian crystalline shield. Oligocene marine basin is a single basin as structural, stratigraphic, and genetic. All separate ore-bearing parts in this basin are parts of a same system in Oligocene basin. The Nikopol Oligocene basin consists of two structural stages, Precambrian crystalline basement rocks and sedimentary cover rocks from the Cretaceous to Quaternary. Nikopol Ore horizon is traced in a thickness varying from several cm to 4.5 m and a single stratum from the west to the eastwards to about 250 km (Fig. 11). Nikopol

manganese ore horizon was separated to three different units; carbonate ore, mixed carbonate-oxide ore, and oxide ore (Fig. 11). As it approaches the paleoshoreline from the open sea, it first shows mixed ores and then completely oxide ores. The oxide ores formed earlier than the carbonate matrix and therefore, they were corroded and filled by the carbonate matrix (Fig. 11). The oxide ores can contain the concretion or earthy masses bigger than 25 cm, sometimes with remnants of carbonate or carbonate-oxide textures. The main minerals of the oxide zone are: manganite, pyrolusite, and psilomelano. The principal carbonate minerals are manganocalcite and rhodocrosite. MnO contents of the Nikopol manganese oxide-hydroxide deposit have the highest values, except for the Binkilic, Koryu and Hinode deposits. Fe_2O_3 contents have similar values with Chiatura and Binkilic manganese. Trace element contents of the Nikopol deposit are higher values than in most of these other manganese deposits, and but, lower than in the Chiatura, Binkilic and Elazig manganese deposits especially in terms of Co, Ni, Cu, Sr, Ba and As. The ΣREE values of the Nikopol manganese oxide ores change between 60 ppm and 197 ppm with an average of 108 ppm. The Y concentrations vary from 9.1 to 47.1 with average of 18.2 ppm. The PAAS-normalized REE +Y patterns of these samples followed similar trends to each other and are characterised by a general increase in normalised concentrations along the series, from light REE to heavy REE (Fig. 8). The average REE sequence in the PAAS-normalized REE pattern for the Nikopol manganese oxide-hydroxide ores is as follows: MREE (3,59) > HREE (3.04) > LREE (2,13). The La_n/Yb_n ratios of the Nikopol manganese oxide-hydroxide ores ranged between 0.68 and 1.06 with a mean of 0.86, verifying the MREE and HREE enrichments. In addition, when compared to PAAS-normalized REY pattern of different environments reported by Bau et al. (1997), the Nikopol manganese oxide ores have similar pattern to hydrogenetic Fe-Mn nodules (Fig. 11). The Ce/Ce* values of manganese oxide-hydroxide ores collected from the study area vary from 0.88 to 1.43, with the mean of 1.16. Most of manganese samples have positive Ce anomalies except for a few samples, indicating that ore-forming rocks were primarily marine chemical or biogenic deposit. Local positive Ce anomalies in some modern dissolved Mn-rich develops beneath the Mn (IV/II) redox cline (De Carlo and Green, 2002; De Baar et al., 1988; Bau et al., 1997). This positive Ce anomaly has been reported to occur in late Ediacaran carbonates (Mazumdar et al., 2003), cherts and Fe formations from the Palaeoproterozoic (Slack et al., 2007). This is more likely to inheritance from mineralization of a Mn oxide-hydroxide. Ce anomalies are used as a common redox proxy to speculate on the oxygenation of the marine environment during the Phanerozoic or Precambrian anoxic events (Liu et al., 1988; Bodin et al., 2013; Riding et al., 2014; Tostevin et al., 2016). All these data indicate that the Nikopol manganese deposit formed in an environment where increase/decreases in fO_2 and pH or increase in temperature in compared to similar environments, low-oxygen fugacity in source of the hydrothermal fluids, volcanogenic input or hydrothermal contributions to seawater, and high Co, Ni, Cu, Sr, Ba and As and low V, Rb, Nb, Hf, U, Th, Pb and Zn values. Maynard (1983) reported that Oxide and nodules in the Nikopol ores had more Ni, Cu, Co, V concentrations than in mixed and carbonate ores in Nikopol manganese deposit. This indicates that the hydrothermal fluids played an important role in the formation of manganese mineralization, especially during the formation of the oxide ores. As indicated by Bolton and Frakes (1985), manganese, which resulted from the decomposition of regional rocks with average shell abundance values, was concentrated in a dissolved form in

an oxygen depleted basin during marine transgression. Manganese initially precipitated as oxides and hydroxides ahead of the landward migrating oxidation/reduction interface is largely diagenetically remobilized and eventually concentrated at the shoreline edge where it is precipitated as oxides. Manganese ores were deposited during "transgression" in shallow marine environments. All data show that the oxide-hydroxide ores in Nikopol manganese deposit formed in the upper zones and the mixed and carbonate ores formed in deeper parts of the sea.

All geochemical data show that the Nikopol manganese-oxide ores formed rapidly within oxic/suboxic seawater as reflected by the Ce anomalies close to 1. The mixed oxide and carbonate ores formed at deeper-water depths compared to the oxide-hydroxide ores in the Nikopol region. Also, our results point out that the metals were transported from both terrestrial sources (Pb isotopic data) and a hydrothermal source in deeper water (chemical discrimination diagrams). The metals associated with the Mn-oxide ores likely formed syngenetically through microbially mediated mineralization at water depths deeper than the area where the carbonate-ore deposits formed.

Acknowledgements

This work was financially supported by the Firat University (MF.18.49) for financial supports. I would like to thank to POKROV GOK Mining and Processing Plant (Nikopol) and Chief Geologists Sergey Svietlichnyi and Senior Geologist Konstantin Gogolev (Institute of Geochemistry, Kiev) for helpings and supports during field study in Nikopol.

References

Abedini, A., Calagari, A.A. 2015. Rare earth element geochemistry of the Upper Permian limestone: the Kanigorgeh mining district, NW Iran. Turk J Earth Sci 24:365–382.

Akgul, B. (2015) Geochemical associations between fluorite mineralization and A-type shoshonitic magmatism in the Keban–Elazig Area, East Anatolia, Turkey. J. Afr. Earth Sci. 111, 222–230.

Andrieu, A.S., Honnorez, J., Lancelot, J., 1998. Lead isotope compositions of the TAG mineralization, Mid-Atlantic Ridge, 26°08′N. In: Herzig, P.M., Humphris, S.E., Miller, D.J., Zierenberg, R.A. (Eds.), Proceedings of the Ocean Drilling Program, Scientific Results.

Baturin, G.N., 2009. Geochemistry of ferromanganese nodules in the Gulf of Finland, Baltic Sea. Lith. Miner. Resour. 44 (5), 411–426.

Baturin, G.N., Dubinchuk, V.T., 2009. Composition of ferromanganese nodules from Riga Bay (Baltic Sea). Oceanology 49 (1), 111–120.

Baturin, G.N., 2011. Variations in the composition of ferromanganese concretions of the Kara Sea. Okeanologiya 51 (1), 153–161 (in Russian).

Bau M. 1996. Controls on the fractionation of isovalent trace elements in magmatic and aqueous systems: evidence from Y/Ho, Zr/Hf, and lanthanide tetrad effect. Contrib. Mineral. Petrol. 123, 323–333

Bau, M., Möller, P., 1992. Rare-earth element fractionation in metamorphogenic hydrothermal calcite, magnesite and siderite. Minerol. Petrol. 45, 231–246

Bau, M., Dulski, P., 1996. Distribution of yttrium and rare-earth elements in the Penge and Kuruman iron-formations, Transvaal Supergroup, South Africa. Precambrian Res. 79, 37–55.

Bau, M.,Möller, P., Dulski, P., 1997. Yttrium and lanthanides in eastern Mediterranean seawater and their fractionation during redox-cycling. Mar. Chem. 56, 123–131.

Bau, M., 1999. Scavenging of dissolved yttrium and rare earths by precipitating iron oxyhydroxide: experimental evidence for Ce oxidation, Y-Ho fractionation, and lanthanide tetrad effect. Geochim. Cosmochim. Acta 63, 67–77.

Bau, M., Schmidt, K., Koschinsky, A., Hein, J.R., Kuhn, T., Usui, A., 2014. Discriminating between different genetic types of marine ferro-manganese crusts and nodules based on rare earth elements and yttrium. Chem. Geol. 381, 1–9.

Ben Othman, D., White, W.M., Patchett, J. 1989. The geochemistry of marine sediments, island arc magma genesis and crust-mantle recycling. Earth Planet. Sci. Lett. 94, 1-21.

Bodin, S., Godet, A., Westermann, S., Föllmi, K.B., 2013. Secular change in Northwestern Tethyan water-mass oxygenation during the late Hauterivian–early Aptian. Earth Planet. Sci. Lett. 374, 121–131.

Bolton, B.R., Frakes, L.A. 1985. Geology and genesis of manganese oolite, Chiatura, Georgia, U.S.S.R. Geol Soc Am Bull 96, 1398-1406.

Bonatti, E., Kraemer, T., Rydel, H., 1972. Classification and genesis of submarine iron–manganese deposits. In: Horn, D.R. (Ed.), Ferromanganese Deposits on the Ocean Floor, Washington, D. C., Natl. Sci. Found, pp. 149–166.

Censi, P., Sprovieri, M., Larocca, D., Aricò, P., Saiano, F., Mazzola, S., Ferla, P., 2007. Alteration effects of volcanic ash in seawater: Anomalous Y/Ho ratios in coastal waters of the Central Mediterranean Sea. Geochem. Cosmochim. Acta 71 (22), 5405–5422.

Censi, P., Randazzo, L.A., Zuddas, P., Saiano, F., Aricò, P., Andò, S., 2010. Trace element behaviour in seawater during Etna's pyroclastic activity in 2001: concurrent effects of nutrients and formation of alteration minerals. J. Volcanol. Geotherm. Res. 193 (1–2), 106–116.

Censi, P., Inguaggiato, C., Chiavetta, S., Schembri, C., Sposito, F., Censi, V., Zuddas, P., 2017. The behaviour of zirconium, hafnium and rare earth elements during the crystallisation of halite and other salt minerals. Chem. Geol. 453, 80–91.

Censi, P., Sposito, F., Inguaggiato, C., Zuddas, P., Inguaggiato, S., Venturi, M., 2018. Zr, Hf and REE distribution in river water under different ionic strength conditions. Sci.Total Environ. 645, 837–853.

Censi, P., Raso, M, Saiano, F., Zuddas,P, Oliveri, E. 2019. Zr/Hf ratio and REE behaviour: A coupled indication of lithogenic input in marginal basins and deep-sea brines. Deep-Sea Res. Part II 164, 216-223.

Chakhmouradian, A.R., Wall, F., 2012. Rare earth elements: minerals, mines, magnets (and more). Elements 8, 333–342

Chen, S.. Yin, X.B., Wang, X.Y., Huang, X., Ma, Y., Guo, K., Zeng, Z.G. 2018. The geochemistry and formation of ferromanganese oxides on the eastern flank of the Gagua Ridge. Ore Geol. Rev., 95, 118-130

Choi, J.H., Hariya, Y., 1992. Geochemistry and depositional environment of Mn oxide deposites in the Tokora Belt, norteastern Hokkaido, Japan. Econ. Geol. 87, 1265–1274.

Crerar, D.A., Namson, J., Chyi, M.S., Williams, L., Feigenson, M.D., 1982. Manganiferous cherts of the Franciscan assemblage: I. General geology, ancient and modern analogues, and implications for the hydrothermal convection at oceanic spreading centers. Econ. Geol. 77, 519–540

De Baar, H.J., German, C.R., Elderfield, H., van Gaans, P., 1988. Rare earth element distributions in anoxic waters of the Cariaco Trench. Geochim. Cosmochim. Acta 52, 1203–1219

De Carlo, E.H., Green,W.J., 2002. Rare earth elements in the water column of Lake Vanda, McMurdo Dry Valleys, Antarctica. Geochim. Cosmochim. Acta 66, 1323–1333

Deng, X.H., Chen, Y.J., Yao, J.M., Bagas, L., Tang, H.S., 2014. Fluorite REE-Y (REY) geochemistry of the ca. 850 Ma Tumen molybdenite-fluorite deposit, eastern Qinling, China: constraints on ore genesis. Ore Geol. Rev. 63, 532–543

Dill, H.G., Hansen, B.T., Weber, B., 2011. REE contents, REE minerals and Sm/Nd isotopes of granite- and unconformity-related fluorite mineralization at the western edge of the Bohemian massif: with special reference to the Nabburg-Wölsendorf District, SE Germany. Ore Geol. Rev. 40, 132–148.

Dosso, L., Hanan, B.B., Bougault, H., Schilling, J.G., and Joron, J.-L., 1991. Sr-Nd-Pb geochemical morphology between 10° and 17° N on the Mid-Atlantic Ridge: a new MORB isotope signature. *Earth Planet. Sci. Lett.*,106:29-43.

Dosso, L., Bougault, H., and Joron, J.L., 1993. Geochemical morphology of the North Atlantic Ridge, 10°-24°N: trace element-isotope complementarity. *Earth Planet. Sci. Lett.*, 120:443-462.

Dubinin, A.V., 2006. Rare Earth Elements in the Ocean. Nauka, Moscow (in Russian with English abstract).

Ehya, F., 2012. Variation of mineralizing fluids and fractionation of REE during the emplacement of the vein-type fluorite deposit at Bozijan, Markazi Province, Iran. J. Geochem. Explor. 112, 93–106.

Elderfield, H. 1988. The oceanic chemistry of the rare-earth elements. *Phil. Transac. Roy. Soc. London* A325, 105–126.

Firdaus, M.L., Minami, T., Norisuye, K., Sohrin, Y. 2011. Strong elemental fractionation of Zr–Hf and Nb–Ta across the Pacific Ocean. Nat. Geosci. 4, 227–230.

German, C.R., Elderfield, H., 1990. Application of the Ce anomaly as a paleoredox indicator: the ground rules. Paleoceanography 5, 823.

German, C.R., Holliday, B.P., Elderfield, H., 1991. Redox cycling of rare earth elements in the suboxic zone of the Black Sea. Geochim. Cosmochim. Acta 55, 3553–3558.

Godfrey, L.V., Mills, R., Elderfield, H., and Gurvich, E., 1994. Lead behaviour at TAG hydrothermal vent field, 26°N, Mid-Atlantic ridge. Mar. Chem., 46:237-254.

Godfrey L.V., White, W.M., Salters, V J.M. 1996. Dissolved zirconium and hafnium distributions across a shelf break in the northeastern Atlantic Ocean. Geochim. Cosmochim. Acta 60, 3995–4006.

Godfrey, L.V., Zimmermann, B., Lee, D.C., King, R.L., Vervoort, J.D., Sherrell, R.M., Halliday, A.N. 2009. Hafnium and neodymium isotope variations in NE Atlantic seawater. Geochem.Geophys. Geosyst. 10, 1-13.

Gultekin AH. 1998. Mineralogical and chemical doses are used to determine the origins of manganese deposits. Geol Eng 50: 39-46.

Gultekin, A.H,, Balcı, N. 2018. Geochemical Characteristics of Sedimentary Manganese Deposit of Binkılıç, Trache Basin, Turkey. J Geol Geophys 7/3, 336.

Hart, S.R., 1984. A large-scale isotope anomaly in the Southern Hemisphere mantle. Nature, 309:753-757.

Hein, J.R., Koschinsky, A., Halbach, P., Manheim, F.T., Bau, M., Kang, J.-K., Lubik, N., 1997. Iron and manganese oxide mineralization in the Pacific. In: Nicholson, K., Hein, J.R., Bühn, B., Dasgupta, S. (Eds.), Manganese Mineralization: Geochemistry and Mineralogy of Terrestrial and Marine Deposits. 123–138.

Hein, J.R., Bolton, B. 1994. Formation of the Chiatura and Nikopol manganese carbonate ores, Georgia and Ukraine. Abstracts, Fermor Lecture Meeting, The Geological Society of London, 26-27 September, 1994, London, UK, p. 12.

Hein, J.R., Mizell, K., Koschinsky, A., Conrad, T.A., 2013. Deep-ocean mineral deposits as a source of critical metals for high- and green-technology applications: comparison with land-based resources. Ore Geol. Rev. 51, 1–14.

Hein, J.R., Koschinsky, A., 2014. Deep-ocean ferromanganese crusts and nodules. In: Holland, H.D., Turekian, K.K. (Eds.), Treatise on Geochemistry, second edition 13. Oxford, Elsevier 273–291.

Hein, J.R., Spinardi, F., Okamoto, N., Mizell, K., Thorburn, D., Tawake, A., 2015. Critical metals in manganese nodules from the Cook Islands EEZ, abundances and distributions. Ore Geol. Rev. 68, 97–116.

Hein, J.R. Konstantinova, N., Mikesell, M., Mizell, K., Fitzsimmons, J.N., Lam, P.J. , Jensen, L.T., Xiang, Y., Gartman, A., Cherkashov, G., Hutchinson, D.R., Till, C.P. 2017. Arctic deep water ferromanganese-oxide deposits reflect the unique characteristics of the Arctic Ocean. Geochem. Geophys. Geosyst., 18, 3771-3800.

Ito, E., White, W.M., Göpel, C. 1987. The O, Sr, Nd and Pb isotope geochemistry of MORB. Chem. Geol., 62, 157-176.

Josso, P., Pelleter, E., Pourret, O., Fouquet, Y., Etoubleaua, J., Cheron, S., Bollinger, C., 2017. A new discrimination scheme for oceanic ferromanganese deposits using high field strength and rare earth elements. Ore Geol. Rev. 87, 3–15.

Koç, S., Özmen, Ö., Öksüz, N., 2000. Kasımağa (Keskin-Kırıkkale) mangan oksit cevherleşmesinin oluşum ortamını tanımlayan jeokimyasal özellikler. MTA Dergisi 122, 107–118 (in Turkish).

Konstantinova, N., Cherkashov, G., Hein, J. R., Mirão, J., Dias, L., Madureira, P., & Kuznetsov, V., 2017. Composition and characteristics of the ferromanganese crusts from the western Arctic Ocean. Ore Geology Reviews, 87, 88–99.

Kuleshov, V. 2017. Isotope Geochemistry. The origin and formation of manganese rocks and ores. Elsevier Amsterdam, Netherlands 427p.

Lavelle, J.W., Cowen, J.P., Massoth, G.J., 1992. A model for deposition of hydrothermal manganese near mid-ocean ridge crests. Journal of Geophysical Research 97, 7413 – 7427.

Lilley, M.D., Feely, R.A., Trefry, J.H., 1995. Chemical and biochemical transformations in hydrothermal plumes. In: Humphris, S.E., Zierenberg, R.A., Mullineaux, L.S., Thomson, R.E. (Eds.), Seafloor Hydrothermal Systems: Physical, Chemical, Biological and Geological Interactions. Am. Geophys. Union, Geophys. Monogr., 91, 369 – 391.

Liu, Y.-G., Miah, M., Schmitt, R., 1988. Cerium: a chemical tracer for paleo-oceanic redox conditions. Geochim. Cosmochim. Acta 52, 1361–1371.

Maynard, J. B., 1983. Geochemistry of sedimentary ore deposits: New York, Heidelberg, Berlin, Springer-Verlag, p. 121-144.

Mazumdar, A., Tanaka, K., Takahashi, T., Kawabe, I. 2003. Characteristics of rare earth element abundances in shallow marine continental platform carbonates of Late Neoproterozoic successions from India. Geochem. J. 37, 277–289

McLennan, S.M., 1989. Rare earth elements in sedimentary rocks; influence of provenance and sedimentary processes. Rev. Mineral. Geochem. 21, 169–200.

Mills, R., Elderfield, H., and Thompson, J., 1993. A dual origin for the hydrothermal component in a metalliferous sediment core from the Mid-Atlantic Ridge. J. Geophys. Res., 98:9671-9681.

Muiños, S.B., Frank, M., Maden, C., Hein, J.R., van de Flierdt, T., Lebreiro, S.M., Gaspar, L.,Monteiro, J.H., Halliday, A.N., 2008. New constraints on the Pb and Nd isotopic evolution of NE Atlantic water masses. Geochemistry, Geophysics, Geosystems 9, 18.

Nicholson, K. 1992. Contrasting mineralogical-geochemical signatures of manganese oxides: guides to metallogenesis. Econ. Geol. 87, 1253–1264.

Okay, A.I., Simmons, M., Özcan, E., Starkie, S., Bidgood, M. & Kylander-Clark, A.R.C., 2020, Eocene-Oligocene succession at Kıyıköy (Midye) on the Black Sea coast in Thrace. Turkish Journal of Earth Sciences, 29, 139-153.

Oygür, V., 1990. Çayırlı (Ankara-Haymana) manganez yatağının jeolojisi ve kökeni üzerine görüşler. MTA Dergisi 110, 29–44 (in Turkish).

561 Riding, R., Fralick, P., Liang, L., 2014. Identification of an Archean marine oxygen oasis. Precambrian Res. 251, 232–237.
562 Roy A, Chakrabarti G, Shome D. 2018. Geochemistry of the Neoproterozoic Narji limestone, Cuddapah Basin, Andhra
563 Pradesh, India: implication on palaeoenvironment. Arab J Geosci 11, 784–796
564 Sasmaz, A., Turkyılmaz, B., Ozturk, N., Yavuz, F., Kumral, M. 2014. Geology and geochemistry of Middle Eocene Maden
565 complex ferromanganese deposits from the Elazığ-Malatya region, eastern Turkey. Ore Geol. Rev. 56, 352–372.
566 Sasmaz A, Kryuchenko N, Zhovinsky E, Suyarko V, Konakci N, Akgul B. 2018. Major, trace and rare earth element (REE)
567 geochemistry of different colored fluorites in the Bobrynets region, Ukraine. Ore Geology Reviews 102, 338-350.
568 Schmidt, K., Bau, M., Hein, J.R., Koschinsky, A. 2014**.** Fractionation of the geochemical twins Zr/Hf and Nb/Ta during
569 scavenging from sea water by hydrogenetic ferromanganese crusts. Geochim. Cosmochim. Acta, 140, 468-487.
570 Schwinn, G., Markl, G. 2005. REE systematics in hydrothermal fluorite. Chem. Geol. 216, 225–248.
571 Selin Y.I., 1984. Stratigraphy and mollusks of the Oligocene of Bolshoi Tokmak manganese ore region. Moscow: Nedra,
572 240 p.
573 Shah, M.T., Moon, C.J. 2007. Manganese and ferromanganese ores from different tectonic settings in the NW Himalayas,
574 Pakistan. J. Asian Earth Sci. 29, 455–465.
575 Sinanoglu, D., Sasmaz, A. 2019. Geochemical evidence on the depositional environment of Nummulites accumulations
576 around Elazig, Sivas, and Eskişehir (Turkey) in the middle Eocene sub-epoch. Arabian J. Geoscie. 12:759.
577 Slack, J., Grenne, T., Bekker, A., Rouxel, O., Lindberg, P., 2007. Suboxic deep seawater in the late Paleoproterozoic:
578 evidence from hematitic chert and iron formation related to seafloor hydrothermal sulfide deposits, central Arizona,
579 USA. Earth Planet. Sci. Lett. 255, 243–256.
580 Sokal, R.R. Rohlf, F.J. 1995. Biometry: The Principles and Practice of Statistics in Biological Research, third ed.. W.H.
581 Freeman and Co, New York, p 887.
582 Strishkov, V., Levine, R.M. 1987. The Manganese Industry of the U.S.S.R. Washington, DC: U. S. Bureau of Mines/U. S.
583 Government Printing Office.
584 Sun, S.-S., 1980. Lead isotopic study of young volcanic rocks from midocean ridges, ocean islands and island arcs. Philos.
585 Trans. R. Soc. London. A, 297:409-445.
586 Strakhov, N.M., Shterenberg, L.E., Kalinenko, V.V. and Tikhomirova, Z.S. 1968. Geochemistry of manganese ore
587 sedimentation, Tr.Geol. Inst. AN SSSR, 185, 495 p. (in Russian).
588 Takahashi, Y., Hirata, T., Shimizu, H., Ozaki, T., Fortin, D., 2007. A rare earth element signature of bacteria in natural
589 waters? Chem. Geol. 244, 569–583.
590 Taylor S. R. and McLennan S. M. 1985. The Continental Crust: Its Composition and Evolution. Blackwell, Oxford.
591 Tobia, F.H. 2018. Stable isotope and rare earth element geochemistry of the Baluti carbonates (Upper Triassic), Northern
592 Iraq. Geosci J 22 (6), 975–987
593 Tostevin, R., Shields, G.A., Tarbuck, G.M., He, T., Clarkson, M.O., Wood, R.A., 2016. Effective use of the cerium
594 anomalies as a redox proxy in carbonate-dominated marine settings. Chem. Geol 438, 146–162.
595 Toth, J.R., 1980. Deposition of submarine crusts rich in manganese and iron. Geol. Soc.Am. Bull. 91, 44–54.
596 Turekian, K.K., Wedepohl, K.H. 1961. Distribution of elements in some major units of earth's crust. Geol Soc Am Bull 72,
597 175–192.
598 Varentsov, I.M.1964. Sedimentary Manganese Ores. Elsevier. Amsterdam
599 Varentsov, I. M., and Rakhmanov, V. P., 1977. Deposits of Manganese. In Smirnov V.I. (ed.), Ore Deposits of the USSR,
600 Vol. 1, 114-178 Pitman, London.

Varentsov, I. M., and Rakhmanov, V. P., 1980. Manganese deposits of the USSR (A review), *in* Varentsov, I. M., and Grasselly, GY., eds., Geology 319-391

Varentsov, I.M. 2002. Genesis of the eastern Paratethys manganese ore giants. Impact of events at the Eocene/Oligocene boundary. Ore Geology Reviews 20: 65-82

Vereshchagin, O. S., Perova, E. N., Brusnitsyn, A. I., Ershova, V. B., Khudoley, A. K., Shilovskikh, V. V., Molchanova, E.V. 2019. Ferro-manganese nodules from the Kara Sea: mineralogy, geochemistry and genesis. *Ore Geol. Rev*. 106, 192–204.

von Blanckenburg, F., O'Nions, R.K., Hein, J.R. 1996. Distribution and sources of pre-anthropogenic lead isotopes in deep ocean water from Fe-Mn crusts, Geochim. Cosmochim. Acta, 60, 4936– 4957,

von Blackenburg, F., Nägler, T.F., 2001. Weathering versus circulation-controlled changes in radiogenic isotope tracer composition of the Labrador Sea and northAtlantic deep water. Paleoceanography 16, 424–434

Wang, C.M., Deng, J., Carranza, E.J.M., Lai, X.R., 2014. Nature, diversity and temporal–spatial distributions of sediment-hosted Pb–Zn deposits in China. Ore Geol. Rev. 56, 327–351

Zeng, Z., Ouyang, H., Yin, X., Chen, S., Wang, X., Wua, L., 2012. Formation of Fe–Si–Mn oxyhydroxides at the Pacmanuss hydrothermal field, Eastern Manus Basin: mineralogical and geochemical evidence. J. Asian Earth Sci. 60, 130–146.

Figure File.

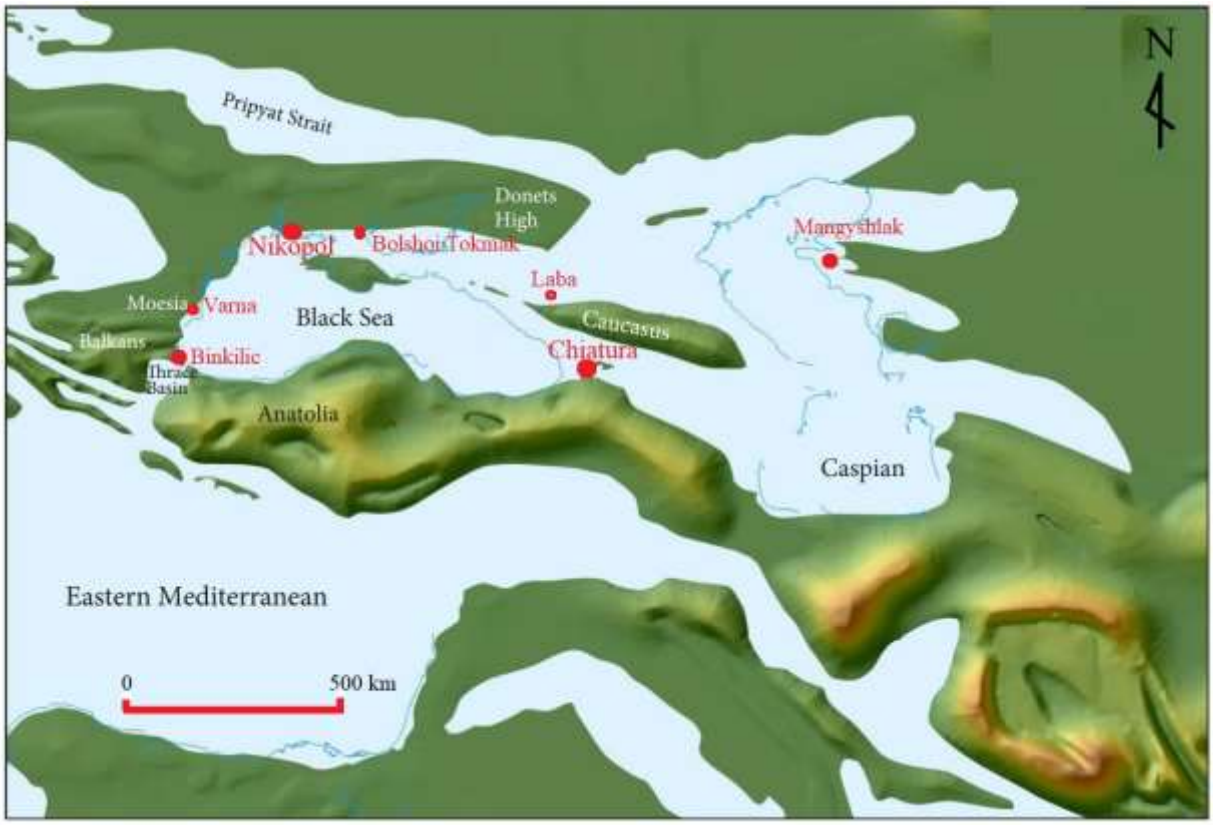

Fig. 1. Map showing location of Chiatura and other Oligocene manganese deposits and simplified regional paleogeography setting of the Early Oligocene of the Eastern Paratethys (Changed from Okay et al., 2020).

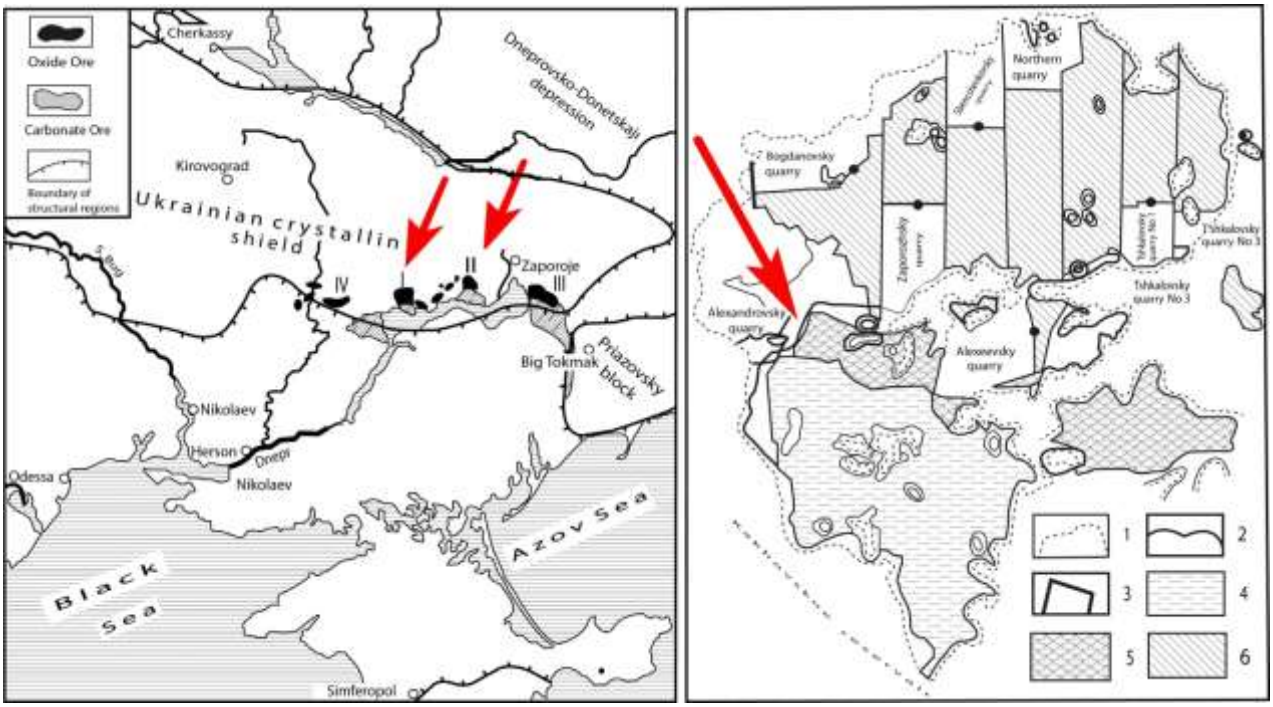

Fig. 2. Structural position of Mn deposits in the Nikopol ore basin (Selin, 1984); 1—boundary of ore bodies; 2—isoline of thickness 0.75m. ore body; 3—boundaries of mining areas; 4—carbonate, 5—oxide-carbonate, 6—oxide.

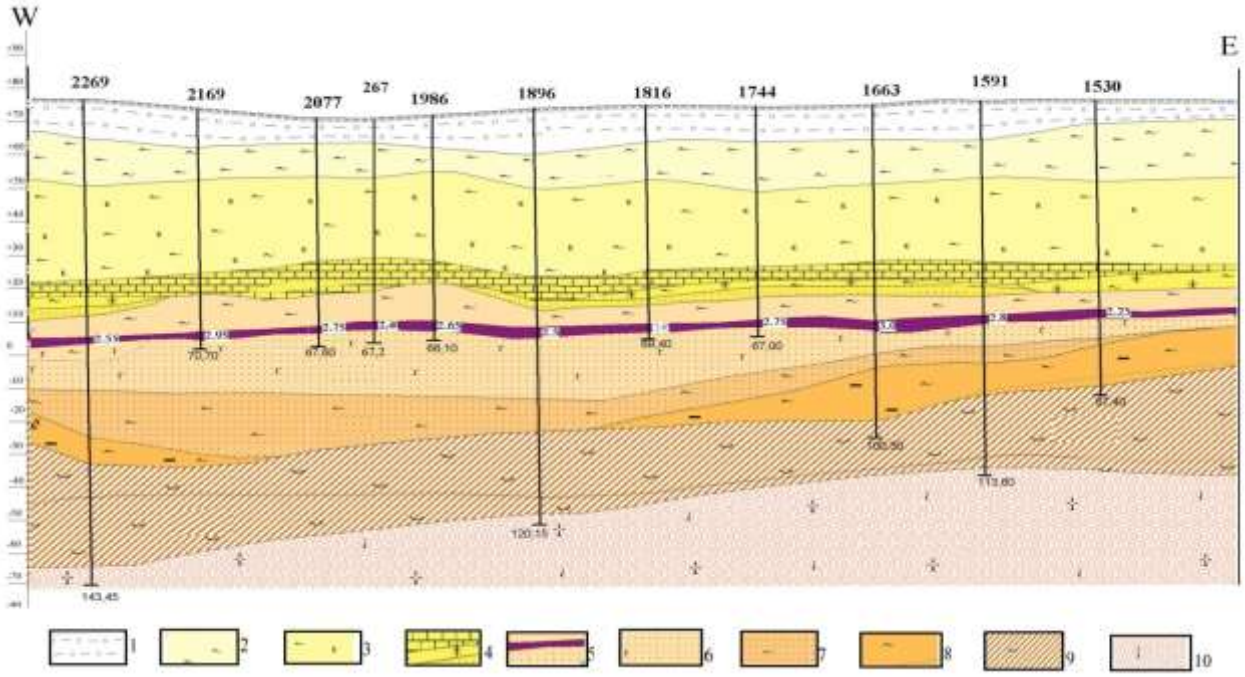

Fig 3. Geological cross section of Nikopol manganese deposit (Strakhov et al., 1968; taken from Kuleshov, 2017); 1—loam; 2—red-brown clay; 3—dark-gray clay; 4—shell limestone; 5—calcareous clay, quartz sand and Mn ores; 6— quartz-glauconite sand; 7— carbonaceous clay and sand; 8—clay interbedded with marl; 9— the weathering crust in crystalline rocks; 10— migmatite and plagiogranite.

Fig. 4. Oxide-hydroxide ore zone in Nikopol manganese deposit

Fig. 5. Oxide-hydroxide ores (black) in mixed oxide-carbonate ore zone

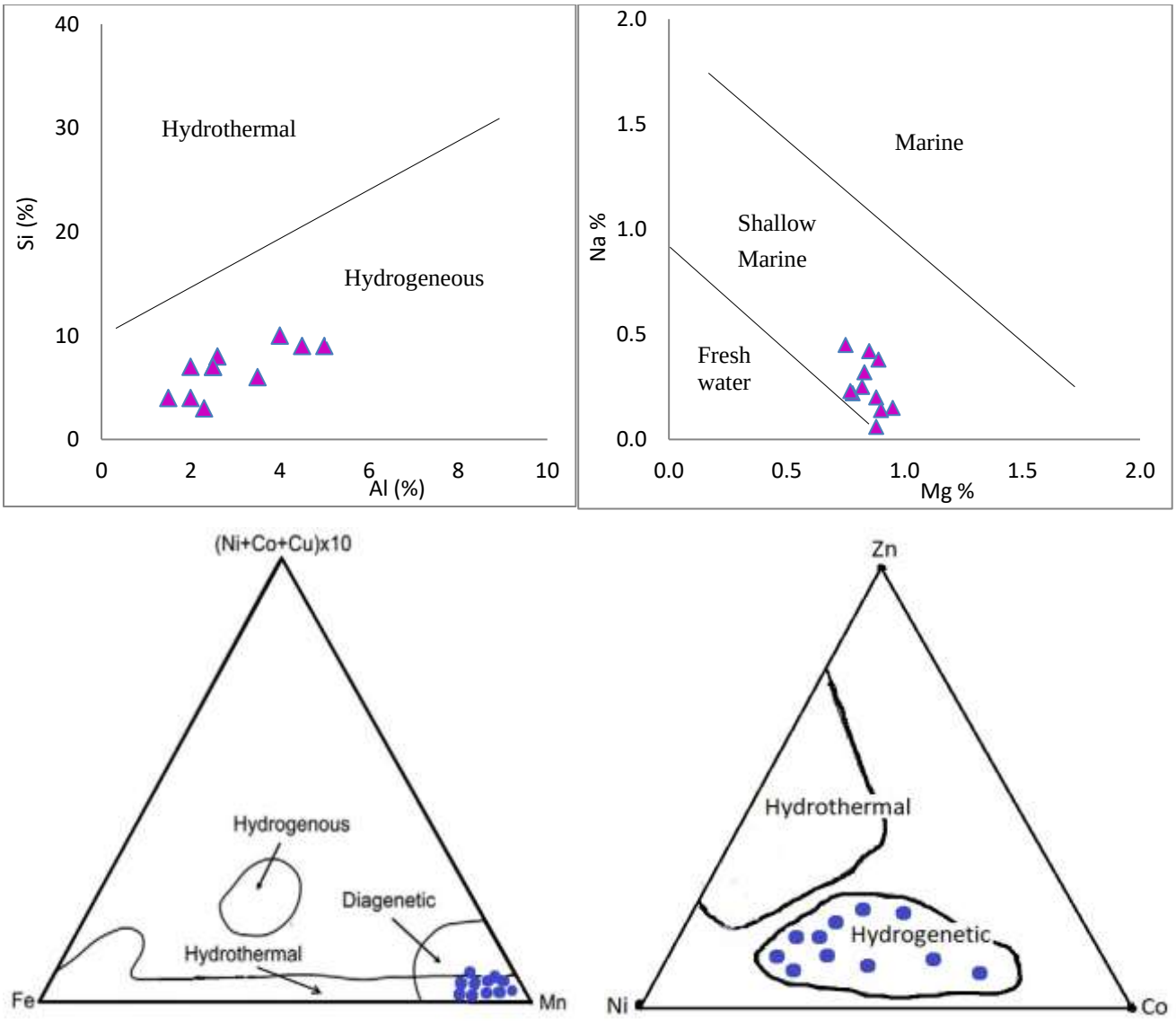

Fig. 5. Discrimination diagrams for the Nikopol manganese oxides Al-Si (Choi and Hariya, 1992), Mg-Na (Nicholson, 1992), Mn–Fe–(Ni + Co + Cu)x10 (Bonatti et al., 1972; Crerar et al., 1982) and Ni–Zn–Co (Choi and Hariya, 1992).

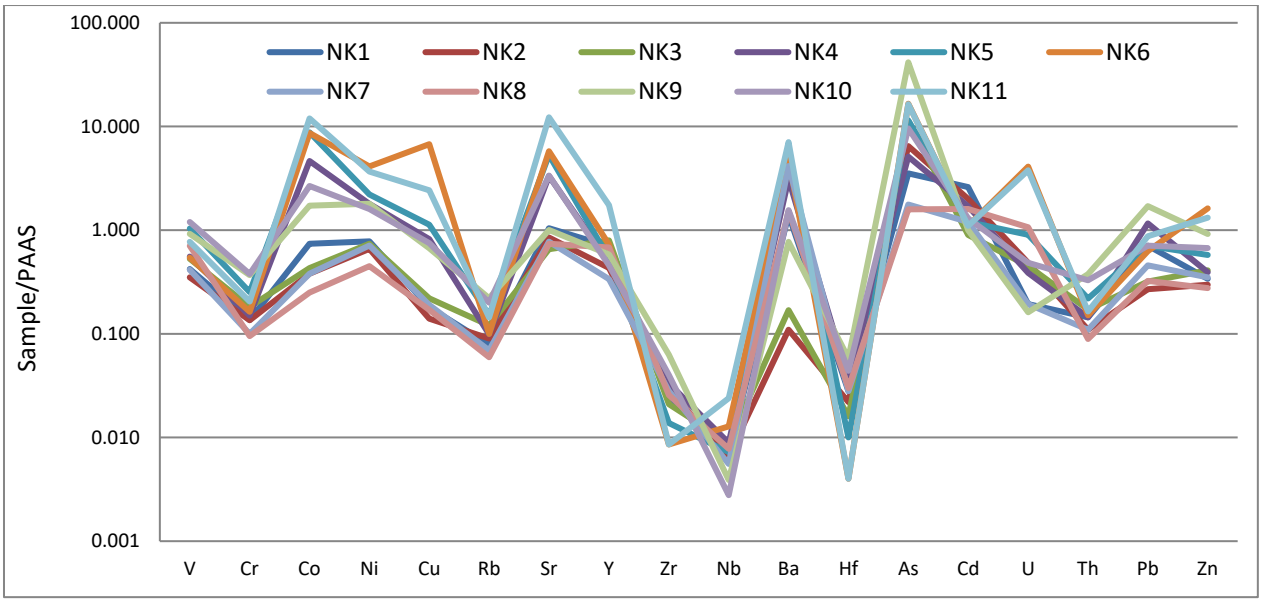

Fig. 6. Post Archean Australian Shale (PAAS)-normalized trace element distribution of Nikopol manganese oxides; PAAS data from Taylor and McLennan (1985).

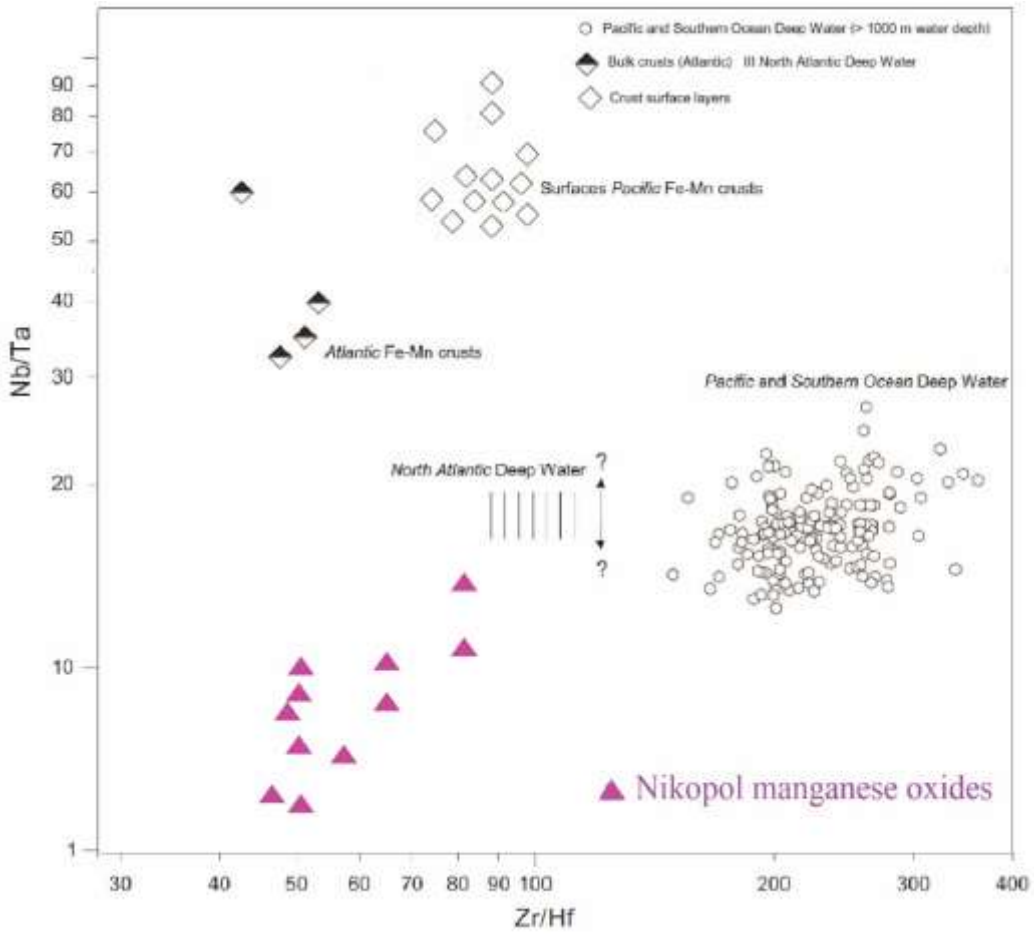

Fig. 8. Nb/Ta and Zr/Hf ratios in Nikopol manganese oxides compared to other oxide deposits (modified from Schmidt et al., 2014; North Atlantic Deep Water, Godfrey et al., 1996, 2009; Arctic and Pacific Deep Water, Firdaus et al., 2011).

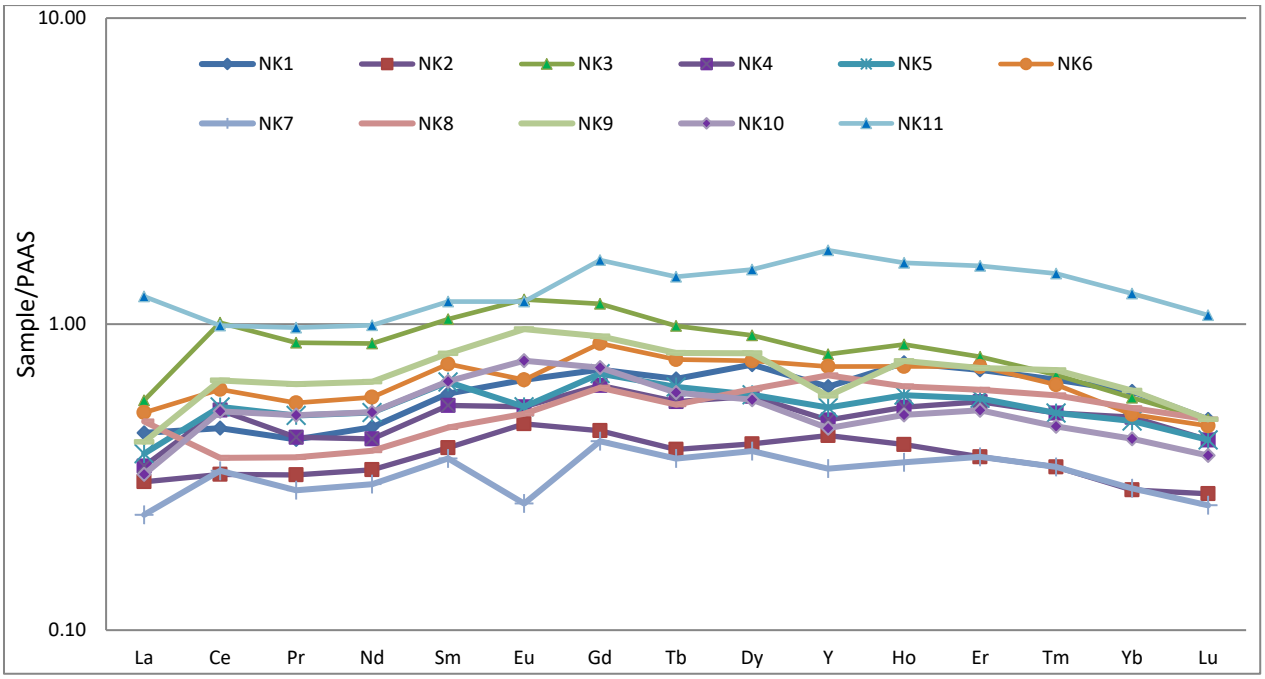

Fig. 8. PAAS normalized REE + Y patterns of the Nikopol manganese samples; PAAS composition from Taylor and McLennan (1985).

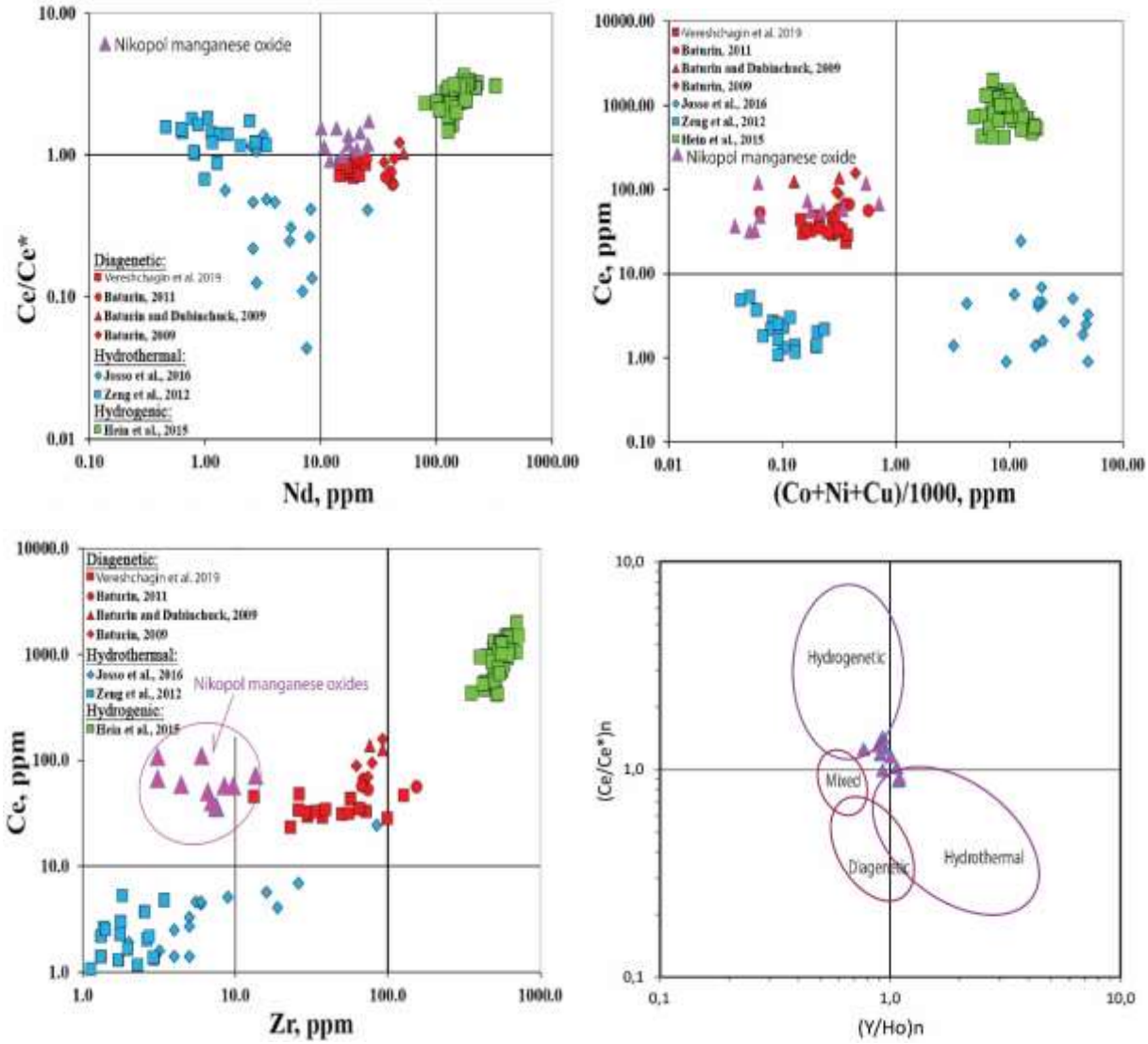

Fig. 9. Different genetic types of Mn deposits in a) Ce/Ce* ratio *vs* Nd concentration (after Bau et al., 2014; Baturin, 2009, 2011; Baturin and Dubinchuck, 2009); b) Ce vs Co+Ni+Co)/1000 ratios, from Zeng et al. (2012), Hein et al. (2015), Josso et al. (2017) and Vereshchagin et al. (2019); c) Ce vs Zr ratios (data in Fig 9a,b,c; from Vereshchagin et al., 2019); and d) Ce/Ce* vs $(Y/Ho)_n$ diagram (from Bau et al. (2014). The ferromanganese concretions of the Kara Sea (Baturin, 2011), ferromanganese nodules in the Gulf of Finland, Baltic Sea (Baturin, 2009), ferromanganese nodules from Riga Bay from Baturin and Dubinchuck (2009) and Ferro-manganese nodules from the Kara Sea (Vereshchagin et al., 2019).

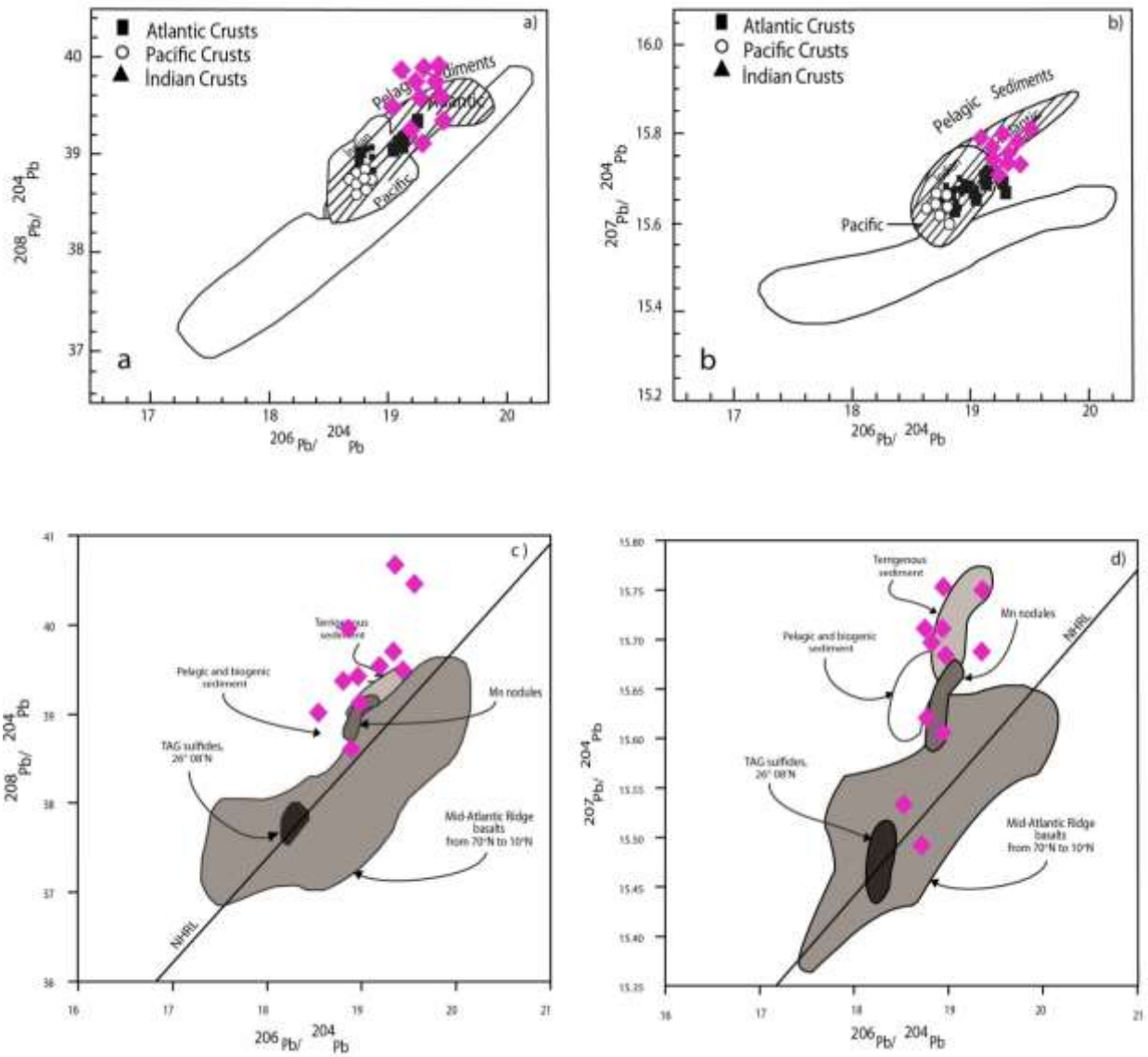

Fig. 10. a) and b) Comparison of Pb isotope ratios for MORB and pelagic sediments with those from Fe-Mn crusts (taken from von Blanckenburg et al., 1996); c and d) diagrams for the Mid-Atlantic Ridge basalts (Sun, 1980; Hamelin et al., 1984; Ito et al., 1987; Dosso et al., 1991, 1993), Atlantic sediments (Ben Othman et al., 1989), and Mn nodules (Ben Othman et al., 1989; Mills et al., 1993; Godfrey et al., 1994). NHRL = the Northern Hemisphere Reference Line according to Hart (1984) (taken from Andrieu et al., 1998).

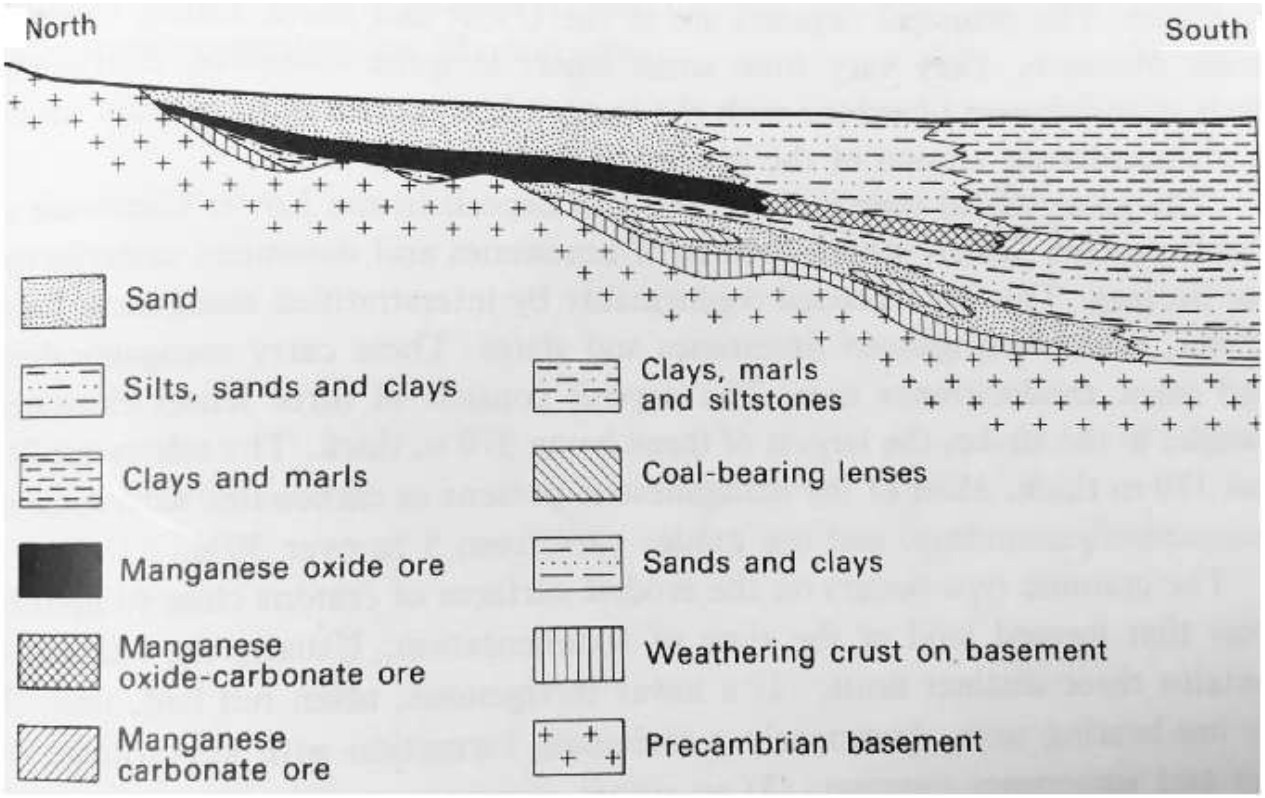

Fig. 11. Cross section through the Nikopol manganese deposit showing the zonation of the manganese ores and transgressive nature of the sedimentary sequence with its overlap on to the Precambrian basement of the Ukrainian Platform (after Varentsov, 1964)

Table 1. Major oxide contents (%) of Nikopol manganese oxide ores.

Sample	SiO_2	Al_2O_3	Fe_2O_3	MgO	CaO	Na_2O	K_2O	TiO_2	P_2O_5	MnO	Cr_2O_3	LOI	Sum	Mn	Fe	Mn/Fe	Al	Si
NK1	16,85	3,89	2,91	1,23	9,62	0,46	0,7	0,15	0,33	42,6	0,004	20,4	99,1	33	1,99	16,6	2,07	7,87
NK2	7,46	3,72	3,94	1,27	4,25	0,31	0,61	0,14	0,33	44,4	0,005	32,8	99,2	34,4	2,7	12,8	1,98	3,49
NK3	17,85	3,6	4,48	1,45	8,03	0,25	0,77	0,18	0,66	32,4	0,006	29,3	99,1	25,1	3,07	8,2	1,91	8,34
NK4	15,27	3,25	4,62	1,33	8,34	0,36	0,93	0,17	0,26	36,1	0,005	28,3	98,9	28	3,16	8,8	1,73	7,14
NK5	21,6	5,05	3,63	1,36	6,24	0,67	0,49	0,26	0,38	37,6	0,008	22	99,4	29,2	2,49	11,7	2,69	10,09
NK6	14,08	4,72	3,64	1,35	3,03	0,45	0,88	0,12	1,07	54,5	0,005	14,5	98,3	42,2	2,49	16,9	2,51	6,58
NK7	10,54	2,04	4,53	1,26	10,5	0,08	0,45	0,1	0,26	38,1	0,004	32,1	99,9	29,5	3,1	9,5	1,09	4,93
NK8	9,61	2,73	3,33	1,01	10,3	0,32	0,38	0,09	0,37	38,4	0,004	32,9	99,5	29,8	2,28	13,1	1,45	4,49
NK9	20,7	6,41	4,49	1,35	7,1	0,2	1,55	0,38	0,24	36,1	0,01	21,2	99,7	28	3,08	9,1	3,41	9,67
NK10	20,97	6,88	3,76	1,28	4,21	0,55	1,88	0,4	0,19	40,7	0,01	18,5	99,4	31,6	2,58	12,3	3,66	9,8
NK11	16,47	3,59	5,73	1,22	6,16	0,57	1,12	0,17	2,29	46,9	0,006	14,8	99,1	36,3	3,92	9,3	1,91	7,7
Avrg	**15,58**	**4,17**	**4,10**	**1,27**	**7,07**	**0,38**	**0,89**	**0,20**	**0,58**	**40,7**	**0,006**	**24,3**	**99,2**	**31,5**	**2,805**	**11,67**	**2,22**	**7,28**

Table 2: Trace element concentrations (ppm) of Nikopol manganese deposit (TTE: Total trace element).

	V	Cr	Co	Ni	Cu	Rb	Sr	Y	Zr	Nb	Ba	Hf	As	Cd	U	Th	Pb	Zn	TTE	Mn/Fe	Co/Ni	Co/Zn	Zr/Hf	Co+Ni+Cu	(Ni+Co+Cu)*10	Nb/Ta
NK1	59	13,6	14,8	43,6	8,9	12,6	209	18,9	5,0	0,13	895	0,14	6,0	0,26	0,6	2,1	14,2	28,8	1333	6,2	0,34	0,51	35	543	673	6,5
NK2	49	13,5	7,6	39,4	7,10	14,4	170	11,7	6,0	0,12	70	0,11	11,0	0,20	1,5	1,6	5,4	25,3	433	6,5	0,19	0,30	54	305	541	3,0
NK3	74	18,2	8,6	44,1	10,9	19,3	131	21,5	4,4	0,16	108	0,08	19,1	0,09	1,4	2,5	6,4	34,8	504	9,5	0,20	0,25	75	668	636	5,3
NK4	78	15,0	93,0	107	41,2	15,8	664	13,1	7,0	0,16	1974	0,18	8,7	0,17	1,2	2,1	23,2	33,4	3078	35	0,87	2,78	62	631	2413	8,0
NK5	145	25,3	176	132	56,6	24,1	1065	14,4	2,9	0,13	3081	0,05	19,5	0,12	2,8	3,2	14,1	49	4811	39	1,32	3,58	70	357	3646	6,5
NK6	76	16,3	173	246	337	15,9	1152	19,6	1,8	0,23	3085	0,02	28,2	0,11	12,7	2,2	12,6	138	5318	15	0,70	1,25	70	1472	7566	7,7
NK7	58	10,0	7,5	42,5	9,57	11,1	155	9,10	5,9	0,10	2644	0,14	3,0	0,12	0,6	1,6	9,2	29,8	2997	38	0,18	0,25	58	446	596	3,3
NK8	99	9,5	4,9	26,8	8,26	9,5	148	18,4	5,4	0,14	973	0,15	2,7	0,16	3,3	1,3	6,5	23,5	1340	43	0,18	0,21	45	1006	400	7,0
NK9	129	36,8	34,3	108	33,6	35,3	201	15,7	13,2	0,07	491	0,29	70,7	0,10	0,5	5,5	34,1	78	1287	47	0,32	0,44	83	745	1758	2,3
NK10	168	37,7	53,4	96,6	37,6	32,0	673	12,3	8,4	0,05	991	0,22	16,3	0,13	1,5	4,8	14,2	57	2205	26	0,55	0,94	33	320	1876	2,5
NK11	108	20,5	239	221	121	23,0	2453	47,1	1,8	0,43	4491	0,02	27,9	0,11	11,7	2,4	17,5	112	7897	10	1,08	2,13	43	296	5804	14,3
Average	94,8	19,7	73,7	101	61,1	19,4	638	18,4	5,62	0,16	1709	0,13	19,4	0,14	3,44	2,66	14,3	55,4	2836	25	0,54	1,15	57	617	2355	6,0
PAAS	140	100	20	60	50	160	200	27	210	18	636	5	1,7	0,1	3,1	14,6	20	85								

Table 3. Major and trace element contents of various types of manganese deposits. Analyses taken from (1) = (Shah and Moon, 2007), (2, 3, 4, 5) = (Choi and Hariya, 1992), (6) = (Gultekin and Balcı, 2018), (7) = (Oygür, 1990), (8) = (Koç et al., 2000) and (9)= (Sasmaz et al., 2014).

Countries	Pakistan (1)	Japan (2)	Japan (3)	Japan (4)	Japan (5)	Turkey (6)	Turkey (7)	Turkey (8)	Turkey (9)	This study
Regions	Hazara	Wakasa	Koryu	Hinode	Tokora	Binkılıç	Çayırlı	Kasımağa	Maden Complex	Nikopol
Orig ins	Hydrothermal/ hydrogenous	Hydrothermal	Hydrothermal	Sedimentary	Sedimentary	Sedimentary	Volcano-sedimentary	Volcano-sedimentary	Sedimentary exhalative	Sedimentary
SiO_2 (%)	9,41	58,16	40,56	12,7	32	9,69	63	13,4	24,6	15,9
TiO_2 (%)	0,84	0,04	0,05	0,04	0,91	0,30	0,03	0,10	0,14	0,20
Al_2O_3 (%)	12,5	0,55	0,63	1,27	8,82	1,39	0,65	2,95	3,62	4,17
Fe_2O_3 (%)	20,3	0,92	0,55	0,59	38,3	3,69	0,68	14	33,7	4,10
MnO (%)	33,78	32,5	42,06	67,2	5,22	53,2	29,2	40	11,6	40,7
MgO (%)	0,59	0,19	0,02	0,08	4,04	1,12	0,2	12,7	1,23	1,26
CaO (%)	6,43	4,15	1,65	1,67	8,82	16,6	0,24	6,82	9,78	7,07
Na_2O (%)	0,07	0,04	0,11	0,07	0,82	0,43	0,05	0,06	0,1	0,38
K_2O (%)	0,88	0,1	0,27	0,46	0,26	0,34	0,11	0,19	0,04	0,89
P_2O_5 (%)	3,73	0,1	0,02	0,12	0,62	0,97	0,04	0,08	1,35	0,58
Ba (ppm)	6304	13,79	22126	8,1	99	2125	1229	2719	625	1938
V (ppm)	573	258	211	468	1637	39,8	144	106	874	95
Cr	247	10	7	16	186	13,6	13,7	10	18	20
Co	404	2	118	222	433	73,6	25,2	49,5	68,4	74
Ni	305	28	351	341	432	125	69,4	23	662	101
Cu	375	50	1174	691	500	95,6	154,9	126,8	553	61
Zn	580	26	129	147	374	60	66,7	63,5	288	55,4
Pb	2357	112	14	18	267	41	6,5	53,5	115	14.3
Th	31	2	2	98	4	-	0,4	433	2,45	2,66
Rb	24	2	3	4	5	18	2,9	5	1,62	19
Sr	-	85	483	260	102	2664	243	255	588	638
Y	-	5	-	-	80	14,8	33	22	136	18.4
Nb	-	3	8	4	4	-	0,7	11,1	3,94	0,16
Zr	-	12	62	48	104	49,4	4	26,9	88	5,62

Table 4. Rare earth element contents (ppm) and Pb isotope ratios of the Nikopol manganese oxide deposits.

	Y	La	Ce	Pr	Nd	Sm	Eu	Gd	Tb	Dy	Ho	Er	Tm	Yb	Lu	ΣREE	$(Ce/Ce^*)_n$	$(Eu/Eu^*)_n$	$(Y/Y^*)_n$	$(Pr/Pr)_{nn}$	$(La/Yb)_n$	$(Y/Ho)_n$	$^{208}Pb/^{204}Pb$	$^{207}Pb/^{204}Pb$	$^{206}Pb/^{204}Pb$
NK1	18,9	16,6	38,4	3,87	15,6	3,29	0,71	3,31	0,51	3,45	0,74	2,02	0,27	1,70	0,21	91	0,99	1,03	0,83	0,95	0,73	0,84	39,24	15,72	18,92
NK2	11,7	14,7	25,7	2,84	11,3	2,19	0,51	2,09	0,30	1,90	0,40	1,05	0,14	0,81	0,12	64	1,02	1,12	1,04	0,94	1,06	1,07	39,56	15,68	19,04
NK3	21,5	38,9	80,5	7,68	29,3	5,76	1,30	5,43	0,76	4,30	0,85	2,23	0,28	1,62	0,21	179	1,43	1,09	0,90	1,01	0,98	0,93	38,94	15,65	19,03
NK4	13,1	17,5	41,7	3,77	14,3	3,01	0,58	2,94	0,43	2,72	0,53	1,59	0,21	1,40	0,18	91	1,37	0,93	0,88	0,92	0,69	0,91	39,45	15,64	18,88
NK5	14,4	18,9	42,7	4,44	17,4	3,59	0,58	3,21	0,48	2,75	0,58	1,63	0,21	1,36	0,18	98	1,18	0,81	0,90	0,95	0,78	0,91	39,58	15,66	18,98
NK6	19,6	22,2	48,7	4,88	19,6	4,11	0,71	4,03	0,59	3,55	0,72	2,07	0,26	1,43	0,20	113	1,15	0,83	0,96	0,93	1,01	1,00	38,64	15,67	18,82
NK7	9,1	12,4	26,4	2,53	10,2	2,02	0,28	1,93	0,28	1,80	0,35	1,05	0,14	0,82	0,11	60	1,27	0,68	0,92	0,94	0,82	0,95	38,82	15,73	19,22
NK8	18,4	18,2	29,1	3,24	13,1	2,55	0,55	2,89	0,42	2,87	0,62	1,74	0,24	1,50	0,21	77	0,88	0,96	1,10	0,97	0,90	1,09	39,25	15,66	19,10
NK9	15,7	23,4	52,1	5,62	21,9	4,45	1,04	4,25	0,62	3,76	0,75	2,05	0,29	1,71	0,21	122	1,25	1,18	0,75	0,98	0,68	0,77	39,66	15,70	19,08
NK10	12,3	18,5	41,3	4,45	17,5	3,61	0,82	3,36	0,46	2,65	0,50	1,49	0,19	1,19	0,16	96	1,30	1,12	0,85	0,96	0,77	0,90	39,60	15,69	18,76
NK11	47,1	41,5	78,7	8,60	33,6	6,58	1,28	7,54	1,10	7,06	1,57	4,42	0,60	3,55	0,46	197	0,91	0,86	1,12	0,98	0,98	1,10	39,12	15,71	18,68
Average	18,2	22,3	45,8	4,72	18,5	3,74	0,76	3,73	0,54	3,35	0,69	1,94	0,26	1,55	0,20	108	1,16	0,96	0,93	0,96	0,86	0,95	39,4	15,7	19,0
PAAS	38,2	79,6	8,83	33,9	5,55	1,08	4,66	0,77	4,68	27,00	0,99	2,85	0,41	2,82	0,43	212									